micro

MDPI

Review

Freeform Micro-Optical Elements—Recent Production Techniques, Opportunities and Challenges

Tomasz Blachowicz [1], Guido Ehrmann [2], Johannes Fiedler [3], Reinhard Kaschuba [3] and Andrea Ehrmann [3,*]

[1] Institute of Physics—Center for Science and Education, Silesian University of Technology, 44-100 Gliwice, Poland; tomasz.blachowicz@polsl.pl
[2] Virtual Institute of Applied Research on Advanced Materials (VIARAM)
[3] Faculty of Engineering and Mathematics, Bielefeld University of Applied Sciences and Arts, 33619 Bielefeld, Germany; johannes.fiedler@hsbi.de (J.F.); reinhard.kaschuba@hsbi.de (R.K.)
* Correspondence: andrea.ehrmann@hsbi.de

Abstract

Freeform optics belong to the increasingly important elements in optical research and industry, which pose several challenges regarding design and highly precise manufacturing. First being used in cameras and for focusing, nowadays freeform optics are used in a broad range of applications, from lighting to LiDAR, from endoscopy to photovoltaics, and from astronomical instruments to quantum cryptography. Designing freeform optics can be based on different theories and methods. Fabrication is possible by mechanical methods, such as diamond turning or high-precision milling, often followed by different polishing techniques, as well as laser-based techniques, mainly applying different lithographic techniques. Here, we give an overview of recent design and optimization methods, production methods used during the last years, and applications of freeform optics, including the possibility to combine freeform optics with tunability for different applications. We describe the opportunities of new applications as well as common problems and give an outlook towards future directions of research and development.

Keywords: photopolymerization; tunable micro-optical freeform elements; two-photon polymerization; multiphoton lithography; direct laser writing; diamond turning

1. Introduction

Lenses and other optical parts are used in a broad range of applications, not only in the form of glasses for nearsighted people and microscope lenses, but also in lasers, for lithographic techniques and many other applications [1,2]. Common lenses can be produced by mechanical techniques, such as grinding or lapping [3], by molding [4], or by different 3D printing methods, depending on the used material and the required surface accuracy [5,6].

The growing requirement for freeform optics with improved accuracy, however, has led to the necessity to develop design and production methods further. While a wide range of subtractive manufacturing techniques has been used for the production of freeform optics, such as high-precision turning, milling, fly-cutting and grinding [7,8], nowadays lithographic and additive manufacturing techniques are more and more used.

We present and review the results of our literature search performed in February/March 2026, concentrating on papers indexed in the Web of Science, supplemented by papers found in Google Scholar, mainly from the years 2022–2026. Besides general keywords such as "freeform micro-optics", several specific production techniques and

Academic Editor: Guo-Hua Feng

Received: 28 March 2026
Revised: 4 May 2026
Accepted: 8 May 2026
Published: 11 May 2026

applications were researched, all of which are given in this review as sub-section headers. The combination of a general search with more specific keywords leads to a comprehensive overview given in this review.

This review is structured as follows: Section 2 gives an overview of recent design methods for freeform optics and corresponding theories, followed in Section 3 by the production of freeform optics, subdivided into subtractive, additive and lithographic manufacturing methods as well as finishing procedures. In Section 4, the most recent applications of freeform optics are discussed, before Section 5 gives an overview of the challenges regarding design, manufacturing and metrology, system integration and applications, supplemented by recent research to overcome these problems. Throughout the review, the term "freeform (micro-)optics" refers to (small) optical surfaces that do not have a rotational symmetry, while the term "freeform micro-optical elements" denotes specific optical components on the micrometer scale.

2. Freeform Optics—Mathematical Description and Design

In order to produce freeform optics, it is necessary to describe the required three-dimensional shapes mathematically [9].

Usually, the propagation of light through optical elements is described by Fermat's principle, stating that a ray of light passes between two points in the shortest possible duration, i.e., along the shortest optical length [10], where the optical length is defined as the geometric length times the medium's refractive index. This theory can also explain light reflection on a reflective surface, where incident and reflected rays have identical angles towards the normal direction, while the rays lie in the same plane, and the refraction effect when a ray of light enters a medium with a different refractive index, leading to Snell's law [10].

Extending this simple description of light towards wavefronts of light, emitted from a defined source, Fermat's principle allows for deriving the Malus–Dupin theory, which describes the propagation of a wavefront, where the light rays may experience reflections or refractions [10]. Along this wavefront, all rays—being electromagnetic waves—have the same phase.

While simple lenses are usually described by simple mathematical formulas, they will usually show lens errors, such as spherical and chromatic aberration, coma, or astigmatism. These lens errors can be corrected by combining different lenses, e.g., in a microscope, or by developing new meta-lenses [11–13]. To compensate for time-dependent wavefront deformations, adaptive optics have been developed, in which a deformable optical element is adjusted by real-time calculations to correct for a time-dependent refractive index, as is usually the case in astronomy with earth-bound space telescopes [14–16]. However, deformable mirrors and lenses can also be applied in optical microscopes to improve the resolution and accuracy of imaging [17–19], for wavefront stabilization in lasers [20], and other areas.

Besides deformable optical surfaces, another possibility to adapt optical systems is given by the Alvarez lens [21], similar to the lenses later described by Lohmann [22]. Such lens systems are based on two lenses, which can be laterally shifted to enable varifocal properties, e.g., for inexpensive spectacles [23], but also for fast focusing and other applications [24]. While the first Alvarez lenses were composed of two simple lenses, in recent years researchers also reported Alvarez lenses with freeform optics, as shown in Figure 1.

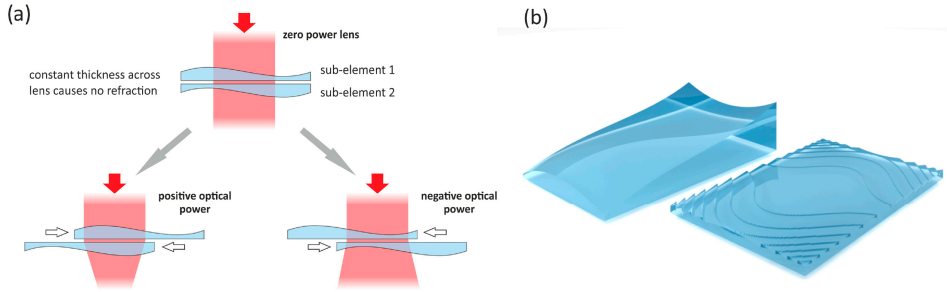

Figure 1. Working principle of the Alvarez lens: (**a**) A modulation of the optical power is attained when conjugate phase plates are shifted with respect to each other in the direction where their phase profile is anti-symmetric. Depending on the displacement of the sub-elements from their zero position, a lens with positive or negative optical power is generated. (**b**) Refractive Alvarez sub-element with a profile function proportional to $x^3/3 + xy^2$ and the corresponding diffractive Alvarez sub-lens, the phase pattern of which is generated by taking the refractive phase structure modulo 2π. From [24], originally published under an Optica open access license.

With increasing complexity of lenses and mirrors, the necessary calculations and design methods to create the desired optical properties also get more and more complex. In addition, it is necessary to investigate the manufacturability of the designed freeform optics, depending on the subtractive or additive manufacturing technique [25–27].

Among the common approaches, ray-mapping methods have to be mentioned, which firstly calculate a ray-mapping from the source to the required irradiance distribution on the target, followed by constructing the necessary surface [28]. These methods, however, necessitate an integrable mapping in order to ensure a continuous surface. As Bösel and Gross have shown, calculation of the mapping is possible for a small-angle approximation by an equation for optimal mass transport [28]. Other approaches are based on the Monge–Ampère methods, i.e., on solving nonlinear partial differential equations of Monge–Ampère type [29], which can be used for single-freeform designs for point sources in a far-field approximation [30] or collimated beams [31]. For the first, the so-called supporting ellipsoids method and its generalization are also suitable [32,33].

Recently, several design concepts have concentrated on miniaturizing the applied illumination concept. Schmidt et al. described a combination of refractive freeform wavefront tailoring and diffractive beam shaping especially for micro-optical systems, leading to so-called freeform holograms [34]. For such miniaturized freeform optics, with characteristic features in the same order of magnitude as the used wavelengths, refractive beam shaping based on a geometrical optical approach becomes problematic, since the wave-optical nature of light has to be taken into account. This is why diffractive beam shaping, which takes into account coherent interference effects between the waves to realize the desired intensity distribution on the target, is advantageous for micro-optics [34].

A design approach for ultra-thin freeform micro-optical elements was suggested by Leiner et al. [35] in order to enable a laser direct writing method to produce freeform optical elements, as opposed to common mechanical methods. While laser direct writing is more cost-effective, it can only produce elements of a limited height, which is why the authors developed a method to design freeform micro-optical elements with a maximum height of 50 µm, which was investigated for the specific example of uniform illumination in ultra-thin direct-lit luminaires. For this, they used a matrix of freeform micro-optical elements with hexagonal irradiance distribution. By implementing secondary triangular target areas and an algorithm for iterative ray-mapping, the overall irradiance distribution became highly uniform [35].

Off-axis reflective systems can be used to enlarge the field of view and to reduce obscuration. On the other hand, they induce different asymmetric aberrations, which

need to be corrected. This leads to the necessity to exchange common surfaces with rotational symmetry by freeform surfaces [36,37]. Freeform surface systems, on the other hand, are problematic to assemble due to the missing rotational symmetry [38]. Xia et al. reported a freeform surface system design method which improved the assembly tolerance requirements of optical systems by about a factor of 2, so that freeform off-axis systems could be realized more easily [39].

Another area in which freeform optics can be used is the creation of optical beams with phase singularities, which is an important tool for high-resolution imaging and advanced microscopy [40,41], optical switching [42,43], and other fields [44]. Among the different methods to create geometric-phase optical elements that can shape optical wavefronts, spatially varying axis plates based on liquid crystals have been investigated in detail [45–47]. Piccirillo et al. showed that dark hollow beams with highly variable-intensity landscapes could be generated by an azimuthal phase factor for optical field encryption, i.e., by directly encoding the required geometric properties into the mold which is used to prepare a liquid-crystal-based freeform waveplate [48].

As these examples show, different mathematical and design approaches are required to define freeform surfaces optimized for the respective application. Besides the theoretical surface shapes, it is necessary to improve the production techniques in order to reduce roughness and waviness of the freeform optics as well as potential material shrinkage and deformation upon thermal and other post-treatments. The next section describes recent subtractive and additive production techniques for freeform optics.

3. Production of Freeform Optics

This section gives an overview of different subtractive and additive production techniques for freeform optics that have been reported in recent years. This classification is based on the different physical processes used: While subtractive processes start from a bulk substrate and remove material to create the designed freeform optics, additive processes form the required shapes by polymerizing material at defined positions. Lithographic methods—that are in the literature sometimes regarded as additive, sometimes as subtractive—are usually based on pattern transfer, e.g., from a mask or digital exposure, and subsequent development or etching. Finishing, as the last sub-section, does not significantly change the geometry of freeform micro-optics, but rather their surface roughness.

3.1. Subtractive Production

Subtractive production techniques, such as turning, milling, fly-cutting or grinding, have been used for the production of freeform optics for a long time. A comprehensive overview of these techniques was given in 2022 by Kumar et al. [8], who described in detail the applicable techniques like ultra-precision diamond turning, ultra-precision milling, ultra-precision fly-cutting, ultra-precision grinding, and the respective state of the art. In addition, they reported the subsequently necessary polishing method, such as bonnet polishing, magnetorheological finishing, laser polishing, and ion beam polishing [8].

In recent years, some new developments have been reported in these and other areas, which are depicted in the following sub-sections.

3.1.1. Diamond Turning

Diamond turning can be used to machine flat, aspheric or also freeform surfaces [8].

Hard and brittle substrates are not easy to machine by diamond turning. One method to overcome this problem is laser-assisted diamond turning [49]. You et al. suggested a special laser-assisted diamond turning method, in which they used a PID laser power controller to optimize the laser heating temperature stability and pre-compensated the

thermal expansion in the toolpath [50]. In this way, they could produce silicon freeform optics without thermal defects.

Zhang et al. concentrated on the problem that a constant control point sampling scheme may lead to losing micro-features [51]. They showed that an optimized sampling pattern could reduce the measured form error by about one third, without increasing the number of control points, as depicted in Figure 2.

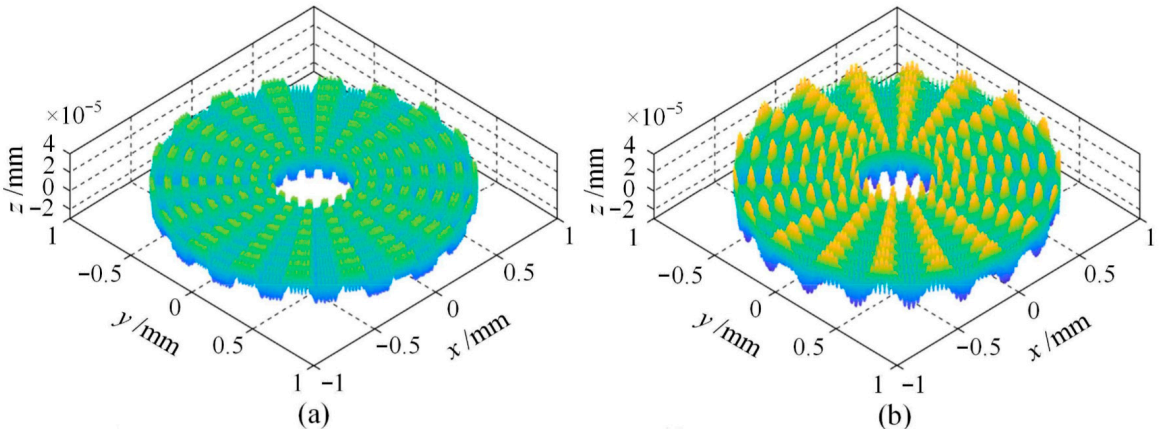

Figure 2. The 3D morphologies of the form error map in the ring pattern in (**a**) the adaptive control point sampling method and (**b**) the constant sampling method. From [51], published under a CC-BY-NC-ND license.

Another way to improve the sampling scheme was suggested in [52], where a toolpath modification based on iterative learning was described, which allowed for producing high-quality freeform surfaces with high efficiency. Here, the focus was on compensating servo dynamic deviations by iterative adjustments. This method especially aimed at mass production and was shown to reduce the form error by approx. 40% to 527 nm for sinusoidal grid surfaces [52].

Working with brittle single-crystal germanium for infrared imaging systems, Prasad et al. reported a method to overcome thermally induced defocus challenges [53]. Applying a hybrid cutting approach, i.e., combining constant-angle and arc cutting, was shown to improve the surface quality to a form error of 0.47 µm and a surface roughness Sa of 2 nm.

For the special case of fast-tool-servo diamond turning of freeform surfaces, Hashimoto and Yan investigated the sources of form errors due to clocking angle errors based on servo control time delays in the system [54]. By carefully identifying and compensating these time delays, they could reduce the form accuracy to 850 nm.

3.1.2. Diamond Milling

Diamond milling uses a tool with a diamond tip, which is fixed on a spindle and rotates with it [8].

Diamond milling, like diamond turning, necessitates proper toolpath planning due to the variational features of freeform optics. Guo et al. developed a feature-adaptive toolpath planning to improve the uniformity of the surface texture [55]. Starting from two different mathematical descriptions of freeform optics for a virtual-reality lens and an LED lens, they used the equal chord length strategy to define the feed distance between neighboring tool location points. After adapting the step distance to surface curvature, tool geometries and machining parameters, they produced freeform optics from oxygen-free copper with a significantly improved surface roughness Sq around 8.5 nm.

Wu et al. also used a freeform LED lens and a virtual-reality lens from oxygen-free copper for their experiments on a five-axis ultra-precision machine [56]. They developed a

process for the surface measuring, here by a white-light interferometer, that combined a coarse registration based on two-dimensional Fourier transform and Pearson correlation coefficient with a fine registration based on singular value decomposition. In this way, they achieved a very low deviation between designed and measured surface after fine registration below 10^{-7} µm.

A semi-ductile diamond milling method was proposed by Li et al., who took into account the full surface curvature variation, microstructure geometry characteristics, and machining parameters [57]. By matching the chip thickness in subsequent tool rotations along the feed direction with the material depth of ductile–brittle transition, while using a constant tool residual height in step direction, the toolpath was planned by an iterative algorithm. This led to a sinusoidal surface roughness Sa of 16 nm, as opposed to 75 nm after conventional diamond milling.

An even lower surface roughness Sa of 4 nm, combined with improved processing efficiency, was reported by Sun et al., who used a self-tuned diamond milling approach for infrared micro-optic arrays [58]. They added a double-axial rapid servo movement platform to the raster milling system in order to match the maximum chip thickness per rotation tool cycle with the critical cut deepness of the infrared material, which not only led to an enhanced surface homogeneity, but also avoided cracks.

It should be mentioned that not only the diamond milling process itself, but also the diamond tools for this process are regularly developed further [59], e.g., by investigating the possibilities of different 3D printing techniques [60] or by using a picosecond laser-based single-crystal diamond tool fabrication technique to prepare micro-milling tools especially for fused silica lenses [61].

3.1.3. Fly-Cutting

Similarly, the machine tools for fly-cutting have a strong impact on the produced freeform optics, such as the tool nose radius and the swing distance [62]. In fly-cutting, a diamond tool on a spindle is used to remove material from a substrate [8]. The process can be differentiated into end fly-cutting and radial fly-cutting, as depicted in Figure 3 [63].

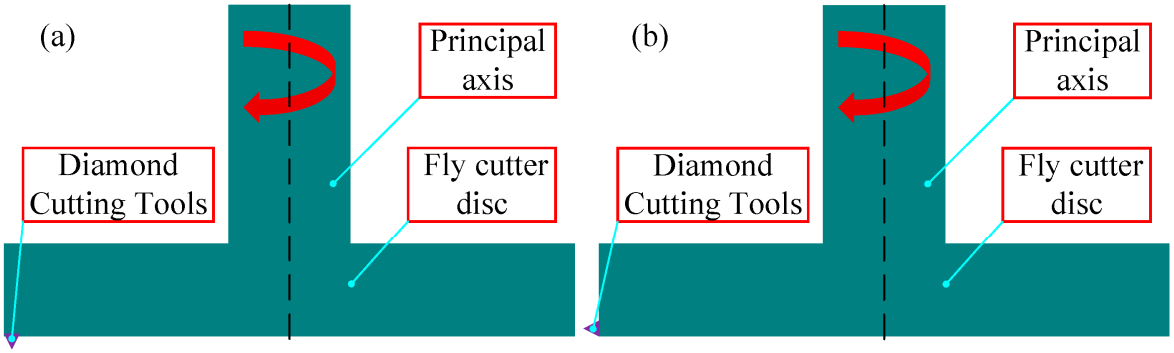

Figure 3. Diamond fly-cutting processing method. (**a**) End fly-cutting. (**b**) Radial fly-cutting. From [63], originally published under a CC-BY license.

Especially for large-scale lens arrays, a new end fly-cutting process was suggested by Zhang et al. who developed a mathematical model for a uniform tool trajectory during production of square and hexagonal boundary lens arrays [64]. They found a root mean square error of less than 1 µm by comparing measured and simulated results.

Bu et al. worked with diamond fly-cutting to produce anti-reflective microgroove arrays on BK7 glass [65]. They investigated the impact of machining parameters and tool geometries on the surface quality and found that sidewall collapse and crack propagation

could be reduced by a higher rotational speed and a lower feed rate, while the tool rake angle had only a very small influence.

In order to produce straight-groove microstructure arrays from shapes like square or triangular pyramids, Wang et al. developed a method to use an ultra-precision machine tool with only three axes, combined with a new offset-tool-servo end fly-cutting system, integrating slow-tool servo technology [66]. For this, they developed a mathematical model to linearize the tool arc trajectories. Comparing theoretical and experimental results, they found a root mean square error below 1 µm.

Generally, fly-cutting is less often used to produce freeform optics than diamond turning, diamond milling, and grinding, which is described in the next sub-section.

3.1.4. Grinding

Grinding is a method of material removal from substrates by a grinding wheel with ultra-fine grains [8].

For large-scale freeform optics, grinding of hard, brittle materials is impeded by the wear of the grinding wheel that is hard to estimate, and by the complicated profile-error measurement directly on the machine. This is why Wang and Zhao concentrated on the development of an on-machine measurement system to improve the effectiveness and machining efficiency of compensation grinding [67]. For this, they measured the full-aperture profile error under different sampling parameters along different raster scanning paths by a measurement system on a four-axis machine tool, leading to a sub-micron variation in the measurement results.

For such freeform optics prepared from hard, brittle materials, researchers from the same working group also developed a slow-tool servo with a diamond grinding wheel [68]. After developing a theoretical model of the scallop height and calculating the profile error due to the diamond wheel centering error, they suggested an improved adjustment method for the grinding wheel position. In this way, they reached a high profile accuracy below 100 nm and a surface roughness Sa around 9–24 nm, depending on the machining parameters and the position on the sample.

Another approach was chosen by Procháska et al., who developed a CAD/CAM grinding process chain applicable for conventional and corrective grinding, which they used for freeform optics from S-BSL7 optical glass, leading to a shape error of 15 µm after conventional grinding and 9 µm for corrective grinding, respectively [69]. They showed that the results produced by corrective grinding of other freeform optics varied by about 20%, indicating the stability of this process.

Peng et al. aimed at a low subsurface damage and a high surface shape accuracy during high-precision grinding of hard, brittle materials [70]. By optimizing grinding and polishing, they managed a root mean square of the surface of around 12 nm, while the subsurface damage was approximately halved from 20 µm to 10 µm.

Combining ultra-fine grinding with plasma-jet polishing, Müller et al. showed especially the impact of different polishing steps, as depicted in Figure 4 [71]. The authors used self-designed Alvarez lenses from fused silica glass as test objects and applied a three-stage grinding process, consisting of a coarse pre-shaping, followed by fine freeform shape generation and finally ultra-fine first surface smoothing on a five-axis machine with spherical diamond grinding tools. After plasma-jet polishing, a roughness Sq below 0.5 nm could be reached.

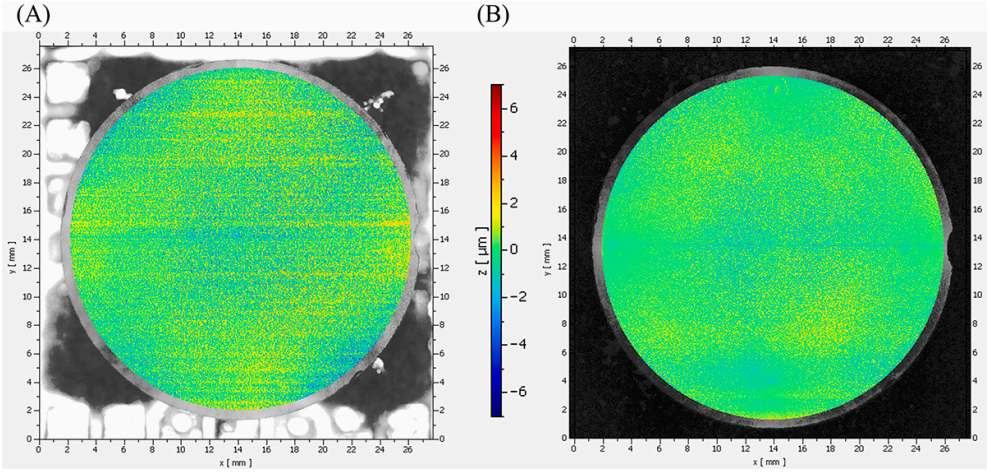

Figure 4. Topographical comparison (figure error topographies) for one Alvarez sample after (**A**) D30 fine grinding and the same sample (**B**) after D16 ultra-fine grinding measured by telecentric WLI. From [71], originally published under a CC-BY license.

3.1.5. Laser-Based Methods

Besides the aforementioned methods of mechanical subtractive manufacturing, freeform optics have also been prepared by laser-based methods, such as selective laser etching (SLE) [72]. In this technique, fused silica and other materials can be shaped on millimeter scales with micrometer precision [73]. As an example, Figure 5 shows the schematic of such a process as well as laser-written tracks from the top and from the side. Using this technique, the authors showed the fabrication of long homogeneous microchannels, to be used as low-loss optofluidic waveguides [74].

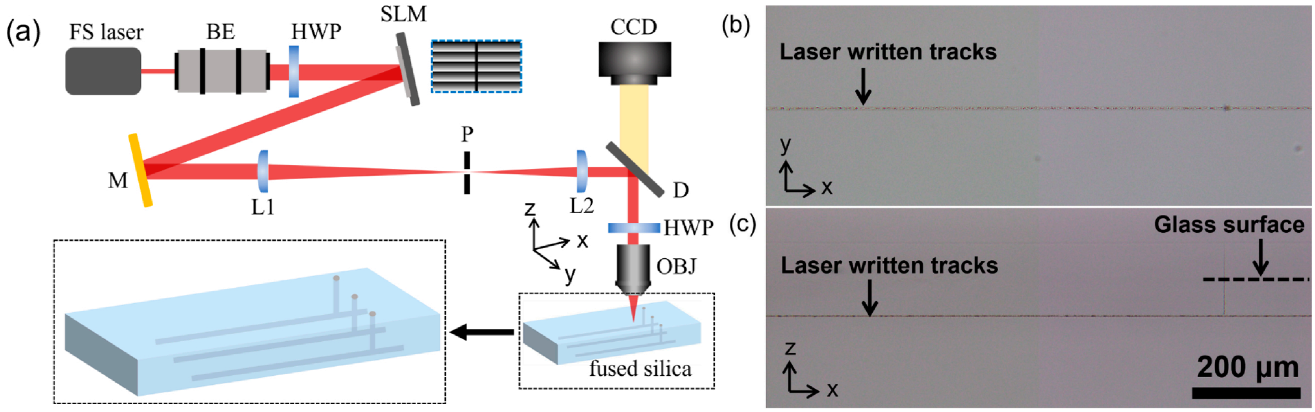

Figure 5. (**a**) Schematic of the spatial light modulator (SLM)-assisted spatially shaped fs laser microfabrication system. The dashed blue rectangle indicates the phase diagram loaded onto the SLM. (HWP: half-wave plate; P: pinhole; OBJ: objective lens; M: metal mirror; D: dichroic mirror; BE: beam expander; L1 and L2 represent lenses with different focal lengths.) (**b**) Top-view and (**c**) side-view optical micrographs of the laser-written tracks inside the fused silica. The dashed line in (**c**) indicates the glass surface. The image below the dashed line in (**c**) shows the actual structure of the laser-written tracks, while the one above the dashed line is a virtual image created by optical microscopy. From [74], originally published under an Optica open access license.

Laser ablation from the front or back surface of a substrate has also been shown by several research groups. Hua et al. used cavitation-assisted ablation by direct laser writing (DLW) with a femtosecond laser on a crystalline substrate and subsequently a high-temperature post-treatment to remove the upper layer which is no longer crystalline due to the ablation process [75]. For this, a low-viscosity liquid was applied at the back of

the crystal substrate, and the laser was focused onto the liquid–crystal interface. The liquid was used to take the ablated debris off the back surface. The final thermal treatment could further reduce the surface roughness Ra from around 21 nm after cavitation-assisted direct writing to around 2.1 nm. This technique was also used for fully three-dimensional nano-sculpturing of different hard materials [76]. Other groups also mentioned the importance of a thermal annealing post-processing step, independent from the exact technique of the previous laser direct writing step [77].

Another parameter which can be optimized for laser ablation is the pulse duration. Zubauskas et al. compared the effect of femtosecond and picosecond pulses regarding the thickness of the removed material and the resulting surface roughness and found that the feature resolution and the surface quality were significantly better for femtosecond pulses, while picosecond pulses enabled higher glass removal rates [78].

While selective laser etching used only a laser to write inside or on the surface of optical materials, Kong et al. combined maskless discrete wet-etching with picosecond laser direct writing [79]. After the laser was used for a line-array discrete modification of the fused silica substrate, hydrofluoric acid was applied for wet-etching along these lines in combination with ultrasonic treatment to form a lens-shaped mold with additional regular surface modifications, which was used to prepare a polydimethylsiloxane (PDMS) lens with an ommatidia-shaped freeform surface. Similar approaches have been reported by other research groups to produce other freeform optics [80–82].

While the previously described methods to prepare diverse freeform optics can be regarded as subtractive techniques, the different lithography processes are usually also subtractive, but sometimes regarded as additive techniques. Thus, an overview of recent lithographic methods to produce freeform optics is given in the next sub-section, followed by a sub-section dealing with conventional additive manufacturing, i.e., 3D printing.

3.2. Lithographic Production

Lithographic methods are used to pattern substrates for diverse sensors and other devices [83]. Recently, different lithography techniques have been applied, depending on the used materials and required resolution, such as optical lithography, extreme ultraviolet (EUV) lithography, electron beam lithography, X-ray lithography, or ion beam lithography, with optical lithography being most often investigated in recent years [83]. Usually, lithography applies light or other electromagnetic waves, projected on a photoresist on top of a wafer or another substrate, to modify the photoresist, as shown in Figure 6 [83]. Afterwards, the photoresist is developed, leading to the exposed areas becoming more/less soluble in case of positive/negative resists [83].

It should be mentioned that multiphoton lithography, also described as direct laser lithography or direct laser writing, can be used to write small structures inside a photoresist without using a photo-mask by polymerizing the photoresist at the laser focal spot and is nowadays more often used for the production of freeform micro-optics [84–86].

Lithography as a production method for freeform optics is reported by many research groups. Lamprecht et al. described a self-developed grayscale laser direct write method based on one- and two-photon absorption lithography that was used to produce freeform micro-optical elements to project a defined light pattern from an LED onto a wall [87]. A similar two-photon grayscale lithography was also applied by Aderneuer et al. who produced freeform micro-optical arrays and found this process to be much faster and result in a higher surface quality than conventional two-photon polymerization [88], as well as by Weinacker et al. who described an iterative pre-compensation of statistical deviations between printed and targeted structures [89], and by Lutey et al. who optimized this process by a data-driven optimization algorithm [90].

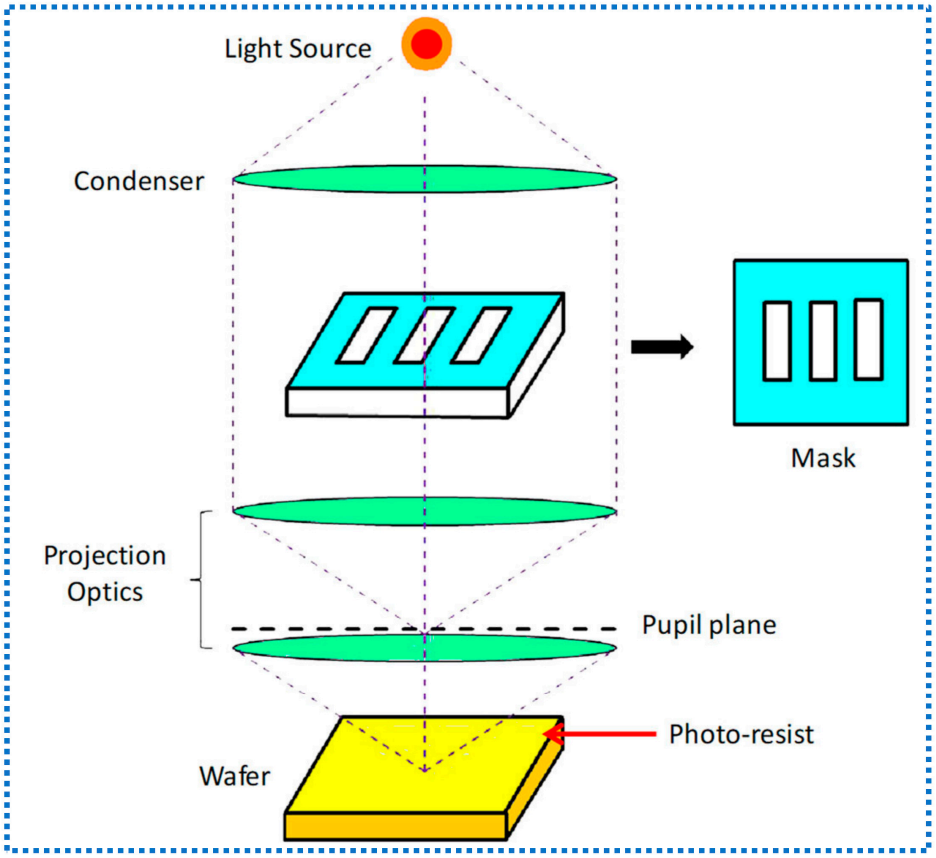

Figure 6. Schematic of optical lithography. From [83], originally published under a CC-BY license.

Leiner et al. used maskless laser direct write lithography, followed by imprinting replication, to produce freeform micro-optical elements with a height of only 50 µm for direct-lit applications [35]. Similarly, Hafttananian et al. suggested a combination of two-photon polymerization by direct laser writing with soft lithography [91], where a stamp or mold from elastomeric PDMS is prepared from the master mold [92]. A combination of multiphoton lithography with atomic layer deposition (ALD) and calcination was suggested by Galvanauskas et al. and Astrauskyte et al. to produce highly transparent, heavy-durability freeform micro-optics [93,94].

A special way of performing lithography was suggested by Toombs et al. who used a microscale computed axial lithography process on fused silica/photopolymer nanocomposites [95]. By using a tomographical 3D illumination of this nanocomposite and subsequent developing in a solvent, they could produce three-dimensional green parts, which were first heated to 600 °C for debinding, followed by sintering at 1300 °C. In this way, they produced a broad variety of different shapes as examples, amongst them freeform micro-optical elements with a surface roughness of 6 nm.

Finally, it should be mentioned that using the subsurface controllable refractive index via beam exposure (SCRIBE) method, it is possible to tune the refractive index of optical components prepared by direct laser writing by applying the DLW process inside nanoporous silicon and silica scaffolds filled with photoresists [96].

3.3. Additive Production

While we gave a broad overview about optical elements from 3D-printed polymers, including the additive manufacturing methods especially suitable for optical elements, in [5], this sub-chapter concentrates on different 3D printing methods which have been applied for the production of freeform micro-optics. Lithographic methods, such as multiphoton

printing [97] or two-photon polymerization [98,99], were described in the previous subsection and are thus not mentioned here again. On the other hand, common 3D printing methods that can be used to print transparent materials, such as stereolitho-graphy (SLA) or digital light processing (DLP), work with visible light and thus cannot produce very fine structures [100]. This would be possible with electron-induced deposition (EID), which, however, has technological limitations leading to a low printing throughput [101].

Nevertheless, some reports of conventional 3D printing methods for freeform optics can be found in the literature. Additive manufacturing of silica glass, e.g., can be performed using sol–gel based materials, in which different organic mixtures contain up to 50% silica nanoparticles, and which can be 3D-printed by SLA, DLP or direct ink writing (DIW) [102]. However, a subsequent sintering step is necessary to get solid, transparent silica glass from the as-printed composite. To solve this problem, Huang et al. suggested crosslinking hydrogen silsesquioxane to silica glass by nonlinear absorption of sub-picosecond laser pulses, resulting in optically transparent glass [102].

Using SLA, Gonzalez-Utrera et al. printed plano-freeform lenses from clear resin [103]. They used isopropyl alcohol to clean the resin excess, followed by washing and curing for 15 min at 60 °C. While the freeform surface was grinded and polished with different micro-graded wet/dry polishing papers, the plane surface was cured whilst pressing it against a flat glass surface (Figure 7). Aiming at an improved resolution while using a low-cost resin printer, Nair S et al. investigated the influence of a fiber-optical taper to demagnify images from the screen of such resin printer, leading to a resolution of around 15 µm half-pitch [104].

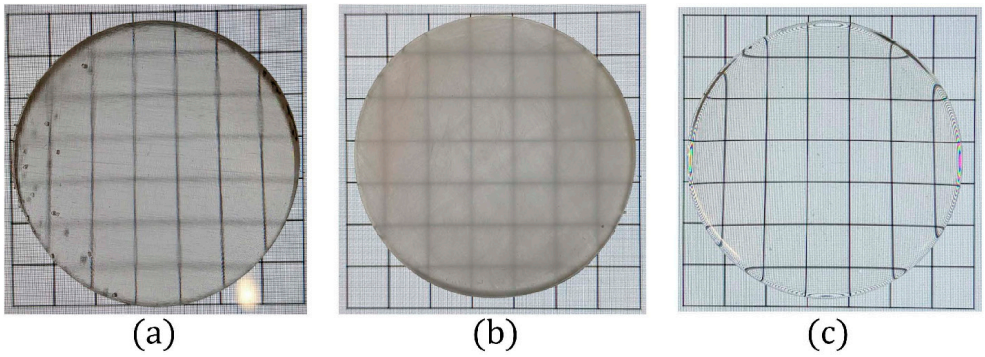

Figure 7. Fabrication process. (**a**) Printing, (**b**) post-processing, and (**c**) polished surface. From [103], originally published under an Optica open access license.

Webber et al. described a modified tomographic volumetric additive manufacturing process [105]. Volumetric additive manufacturing (VAM) is a three-dimensional extension of conventional SLA and DLP printing techniques that build an object layer-wise. In VAM, instead, the whole part is printed at the same time by a tomographic technique. VAM-printed objects still have so-called striation artifacts within the plane of the photoresin vial, resulting in ridges on the object surface. To avoid these artifacts, they suggested using purposely blurred writing beams, leading to strongly reduced striation, as the comparison of VAM-printed microlens arrays in Figure 8b,c shows [105].

Inkjet printing of freeform optics has also been reported in the literature [106]. Williams et al. used inkjet printing for the manufacturing of gradient index optics [107,108]. Sieber et al. applied an optical twin to increase the optical precision by geometrical measurements which were fed back into the simulation model, leading to an optimization of the printing speed, drop size, and UV illumination used for curing [109]. Assefa et al. used a modified inkjet process with three slightly misaligned printheads, containing 1000 parallel nozzles

each, creating layer thicknesses around 4 µm that are solidified by UV exposure, resulting in 3D-printed optical elements that needed no post-processing [110].

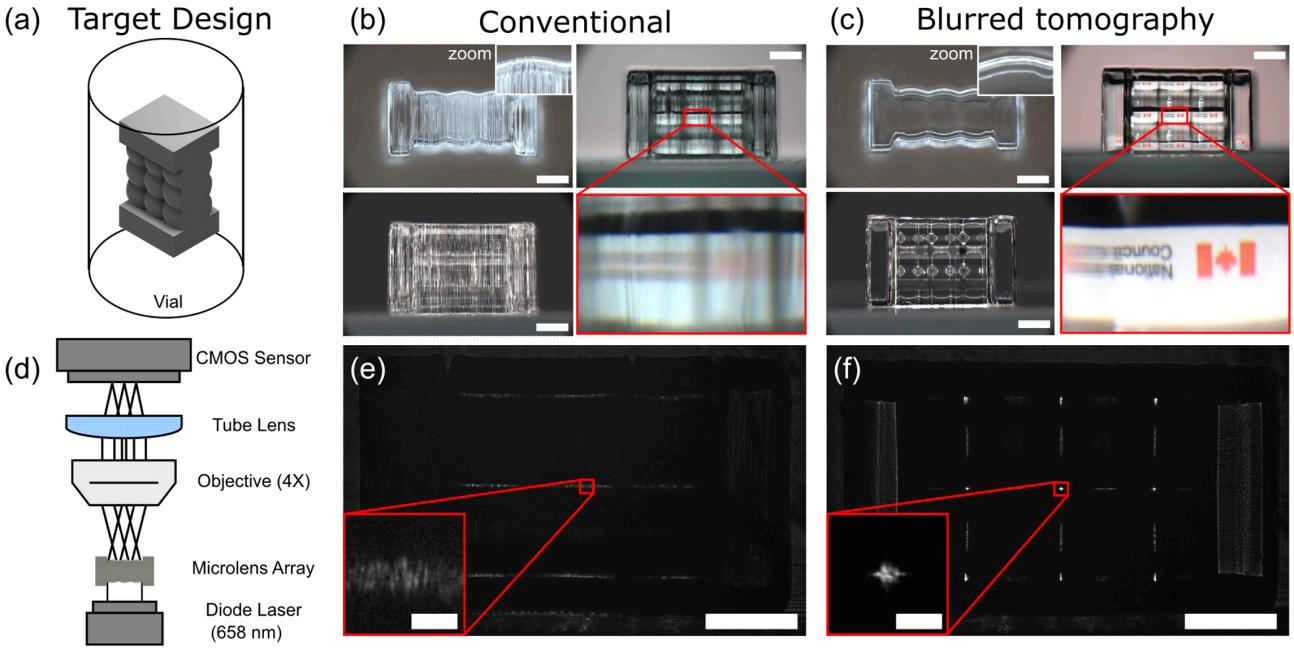

Figure 8. Printing microlens arrays using blurred tomography. (**a**) Computer model of MLA inside vial (not to scale). Images of MLA printed using (**b**) conventional printing conditions and (**c**) blurred tomography. (**d**) Diagram of the setup used to measure laser spot size through the microlens array. Laser spot size measurement of the microlens array printed using (**e**) conventional printing conditions and (**f**) blurred tomography. Scale bars are 1 mm, except insets of (**e**,**f**), which are 50 µm. From [105], originally published under an Optica open access license.

As these few examples show, there are still many kinds of freeform optics that may be 3D-printable by SLA, DLP or inkjet printing, making such freeform optics available also for institutions without specialized lithographic or mechanic machining possibilities.

3.4. Finishing

In most cases, freeform optics are not ready to use after the first production step, but need to be finished, usually by polishing. Typical polishing methods include bonnet polishing, magnetorheological finishing, laser polishing, and ion beam polishing [8]. While these methods are well known, there are nevertheless some papers discussing new aspects.

For bonnet polishing, Deng et al. recently showed that a multi-factor multi-scale material removal function model could be used to reduce the deviation between experimental and theoretical material removal rates [111]. Pant et al. used a seven-axis bonnet polishing machine with polyurethane and uninap-13 pads to polish the surface of a cubic freeform profile, produced by diamond turning [112]. To correct surface shape errors in different bonnet polishing cycles on freeform optics produced by EUV lithography, Peng et al. suggested a cross-scale surface shape error correction method [113].

Magnetorheological (MR) finishing can be combined with chemical finishing by replacing the MR carrier fluid with a reagent, leading to significantly reduced surface roughness [114]. A small polishing wheel especially for micro-optical elements was designed, constructed and tested by Wang et al. who showed that the 13 mm polishing device was better suited for small optical components than a commercial 100 mm device [115]. A robot-assisted magnetorheological finish of freeform surface, based on an industrial 3D

camera, was investigated by Raza et al. who reached a surface roughness of 55 nm after 10 polishing cycles [116].

Laser polishing plays an important role in the finishing of fused silica freeform optics [117]. Metallic freeform optics for EUV applications can also be polished by laser polishing to reach a very low micro-roughness below 0.2 nm root mean square [118]. Laser polishing was also successfully used as post-processing after different laser-ablation methods on quartz glass and Boro-float®33 glass, reducing the surface roughness Ra from around 1 µm to 0.4 µm [119].

In recent years, ion beam polishing of freeform optics has been reported less often in the literature than the other methods, while plasma polishing can sometimes be found as a possible finishing method for freeform optics. The latter can be used for finishing hard–brittle material surfaces, such as glass or fused silica [120]. Fan et al. used multi-jet plasma polishing based on an atmospheric-pressure plasma jet and showed that this method could reduce errors stemming from the periodic toolpath, resulting in a root mean square roughness of 17 nm [121]. Arnold et al. reported even a roughness reduction by three orders of magnitude, depending on the initial roughness, using atmospheric-pressure plasma-jet polishing on fused silica freeform optics [122]. For the investigation of a medium-pressure plasma polishing process on fused silica, Yadav et al. used a comparison of experimental results and numerical simulations to optimize the etchant ratio in terms of surface roughness, at the same time leading to a hydrophilization of the surface [123].

Besides these finishing methods, several other polishing methods can be found in the literature that are more often used on geometric optics than on freeform optics [124].

3.5. Comparative Analysis of Different Production Processes for Freeform Micro-Optics

In addition to the technological descriptions given in the previous sub-sections, here we give a cross-process comparison and discuss the limits of comparability. Generally, such a comparison between different freeform manufacturing techniques is necessary since the performance metrics given in the cited papers depend strongly on the used processes and can often only be applied to a narrow range of techniques [8]. Moreover, different technologies do not only vary in production times, but also in costs, in addition to different quality challenges [125]. Typically, more efficient machining is combined with lower accuracy, while ultra-precision machining needs longer time and has higher costs [55,125]. It should be mentioned that costs do not only increase by increased machining times, but also by tooling, quality tests, etc. [125]. Comparing subtractive and additive production processes, ultra-precision machining has a low throughput, but high flexibility, while lithographic methods have a high throughput at the cost of limited geometric possibilities [8].

As mentioned before, the materials used to produce freeform micro-optics, such as polymers, metals, brittle crystals, etc., limit the machinability, which leads to the problem that not all materials can be manufactured with the same machines. Typically, ultra-precision diamond turning and milling are used for ductile materials, while laser-assisted machining is advantageous for brittle materials [50,126].

In all manufacturing techniques, the process kinematics limit the minimum feature size and thus the achievable surface accuracy. These can be mechanical limitations, such as tool radius or servo bandwidth, or voxel sizes in lithographic and additive manufacturing processes [55,127]. In addition, the necessity to follow the designed shape as closely as possible can in all manufacturing techniques increase the surface roughness and vice versa due to mid-spatial-frequency errors which can reduce the optical performance of manufactured freeform optics [50,128]. This leads to the requirement to characterize freeform surfaces along all frequency bands, not only shape deviations or roughness [128].

Another point that makes the production techniques hard to compare is the necessity of post-processing or finishing processes. Different kinds of polishing and even corrective machining are in some papers part of the result, while other studies concentrate on the first production step, reducing the comparability across different production techniques [128].

As described before, there are currently no unified performance metrics available that would enable a reliable comparison of different freeform micro-optics produced by different techniques [8]. This means, on the other hand, that the literature data cannot be compared with high reproducibility and reliability [55,128]. Table 1 thus can only offer estimated performance metrics that may be biased by the aforementioned problems.

Table 1. Comparison of freeform micro-optic manufacturing technologies. Fly-cutting has approximately equal parameters as diamond milling, as the tool principle is similar.

Parameter Technique	Materials	Feat. Size	Form Accuracy	Roughness SA	Efficiency	Scalability	Post-Processing	Costs
Diamond turning	Metals, polymers, IR crystals [126]	µm (tool radius limited) [51]	~1 µm [50]	1–10 nm [50]	Low [129]	Low/ medium [129]	Often required [50]	High [129]
Diamond milling	Metals, polymers [55]	µm [55]	µm [55]	~10 nm [55]	Medium [55]	Medium [55]	Required [55]	High/ medium [55]
Grinding	Glass, brittle crystals, ceramics [69]	>10 µm, grain size limited [69]	µm–10 µm [69]	>50–500 nm [69]	High [69]	High [69]	Required [69]	Low/ medium [69]
Laser-based	Glass (fused silica), transparent crystals [130]	~10 µm [131]	1–10 µm [132]	~100 nm–µm [132]	Low/ medium [133]	Medium [133]	Required [130]	High [133]
Lithography	Photoresists, polymers [134]	1–5 µm [134]	20–100 nm [134]	10–50 nm [134]	High [134]	Very high [134]	Required [134]	Low/ medium [134]
Additive	Photopolymers, hybrid resins, silica glass (incl. sintering) [135]	1–10 µm (voxel size/ shrinkage) [135]	1–10 µm [135]	0.1–1 µm (layers/voxels [135]	Medium/ high [135]	High [135]	Required [135]	Medium/ high [135]

3.6. Metrology and Characterization of Produced Freeform Micro-Optics

While the previous Table 1 as well as descriptions of production methods for freeform micro-optics have already mentioned parameters such as form accuracy and surface roughness, here we discuss measurement and evaluation of these parameters.

Generally, the lack of a rotational symmetry makes measurements of freeform optics much more complicated than evaluations of conventional optics, mainly due to the complicated mathematical description of the designed surface. The methods often mentioned in the literature are B-spline description and B-spline fitting of the surface, point orthogonal projection and registration parameter optimization [136].

The evaluation of surface deviations is necessary along a broad range of spatial frequencies, as different errors—such as shape deviations and roughness—can occur in different manufacturing methods [128]. However, the surface topographies themselves can influence the results of optical measurement methods, such as laser-based, structured light and photogrammetry-based 3D scanning systems, even if proper cutoff wavelengths are defined [137]. While these methods measure the surfaces themselves, it is also possible to measure the optical performance and potential wavefront errors. Such wavefront-based characterization goes one step further than the comparison of theoretically designed and really manufactured freeform micro-optics, as it also allows for the evaluation of aberrations, e.g., by computer-generated hologram interferometry, typically achieving micrometer-level accuracy in wavefront spacing, or non-null interferometric testing for wavefront deformation correction [138,139].

Other metrology techniques that are specifically used for freeform optics are, e.g., phase measuring deflectometry, which becomes complicated for high local slopes [140], Shack–Hartmann wavefront sensing that also necessitates stitching of scanned areas [141],

or focal-plane wavefront sensing techniques that are especially used for highly complex freeform surfaces where common interferometric methods are insufficient [142].

Finally, alignment tolerances and evaluation at the system level are usually performed by investigating the optical performance and wavefront errors, since only in this way can alignment errors be properly estimated, although combined with the effect of surface errors and optical path differences [138,142].

Generally, metrology of freeform optics lacks standardized evaluation processes, since there are no simple correlations between wavefront aberrations—as the actually important measure—and shape errors, surface roughness, and alignment errors that cause these wavefront aberrations. To make things more complicated, the same surface roughness values can cause different optical performance reductions if their spatial frequency distributions vary, besides the additional problem that these effects are usually wavelength-dependent. Finally, surface measurements themselves, especially if stitching is necessary, can lead to apparent errors that make a comparison between different measurement methods often highly complicated [143,144].

4. Applications

Generally, the potential applications of freeform optics can be subdivided into non-image-forming functionalities, such as light concentration, beam shaping, illumination or optical tweezers, and image-forming ones, such as projection, head-mounted displays, eye implants or cameras. It should be mentioned that this separation is not always clear, e.g., when imaging is performed with non-imaging lenses [145], making the following differentiation into sub-chapters partly subjective. In addition, a large area of application is related to coupling, i.e., fiber-to-chip coupling, chip-to-chip data communication, waveguide coupling, etc. Finally, some applications are based on tunable or actuated freeform micro-optical elements. This section gives examples of recent applications.

4.1. Non-Image-Forming Applications

Light concentration and illumination belong to the typical application of freeform optics. To increase the efficiency of natural light utilization, fiber-optic daylighting systems can be used which can contain freeform optics to increase the coupling efficiency and at the same time improve the uniformity of the illumination in the targeted workplace area [146]. To achieve different light patterns from LEDs, freeform optics can be used to enable customized lighting solutions [147]. For high-brightness LEDs, freeform topologies with multiple convex and concave regions can be used to make sure that in the far field, each point is illuminated by several lens regions to minimize glare [148]. Besides LEDs, photovoltaics can use freeform mirror arrays to produce the required light patterns on solar cells [149–151].

Beam shaping also belongs to the often-reported applications of freeform optics. Freeform optics can, e.g., be used to convert the elliptical Gaussian output of a laser diode into a defined intensity profile at a defined working distance [152,153]. While freeform diffractive optical elements are well suited for beam shaping, tailoring the phase and reducing light scattering losses is still problematic, which is why several groups worked on the optimization of design processes for such freeform elements or on optimization of the whole production process from design to fabrication [154,155]. Recently, "programmable" freeform optics serving as a phase-only spatial light modulator were optimized by an unsupervised learning framework in order to predict high-parameter freeform topologies for freely definable target irradiances [156].

The use of freeform optics for optical tweezers is less often reported. On-chip optical tweezers built with freeform micro-optics were shown to allow for a high degree of freedom

regarding the design of the optical field, including strong intensity gradients to improve trapping and manipulating particles [157]. In the automated design of freeform optical systems, combining ray-tracing with artificial intelligence, light-field-based optical tweezers were used as an example [158]. Using a digital mirror array and a freeform microlens array, a matrix of optical tweezers could be produced to trap and move several particles at the same time [159].

Besides these applications, freeform optics are used in many other non-image-forming applications, such as a combination of laser focusing and Raman scattering collection for Raman spectroscopy [160,161] or microlens arrays for diverse purposes [162–164].

4.2. Image-Forming Applications

Among the image-forming applications of freeform optics, projection belongs to the often-mentioned ones. Pattern projection can be used, e.g., for three-dimensional measurements of object surfaces and shapes, applying hybrid projection systems combining a projection lens and a transmissive freeform to prepare an aperiodic sinusoidal fringe pattern [165]. Ultra-short-throw projectors that enable using large screens in small spaces necessitate freeform mirrors to reduce image distortion and uneven illumination [166]. Even common DLP projection optical systems can be improved by using a freeform surface, resulting in a simplified optical design and improved illumination uniformity and optical efficiency [167].

Head-mounted displays for virtual and augmented reality are among the often-mentioned kinds of projection, especially in case of screens that strongly deviate from simple flat screens [168]. In order to reach a wide field of view, freeform off-axis reflective optical designs can be used with opposite-side oblique projection [169]. For augmented reality displays, projection optics can be significantly reduced in space by using freeform optics, as shown in Figure 9 [170].

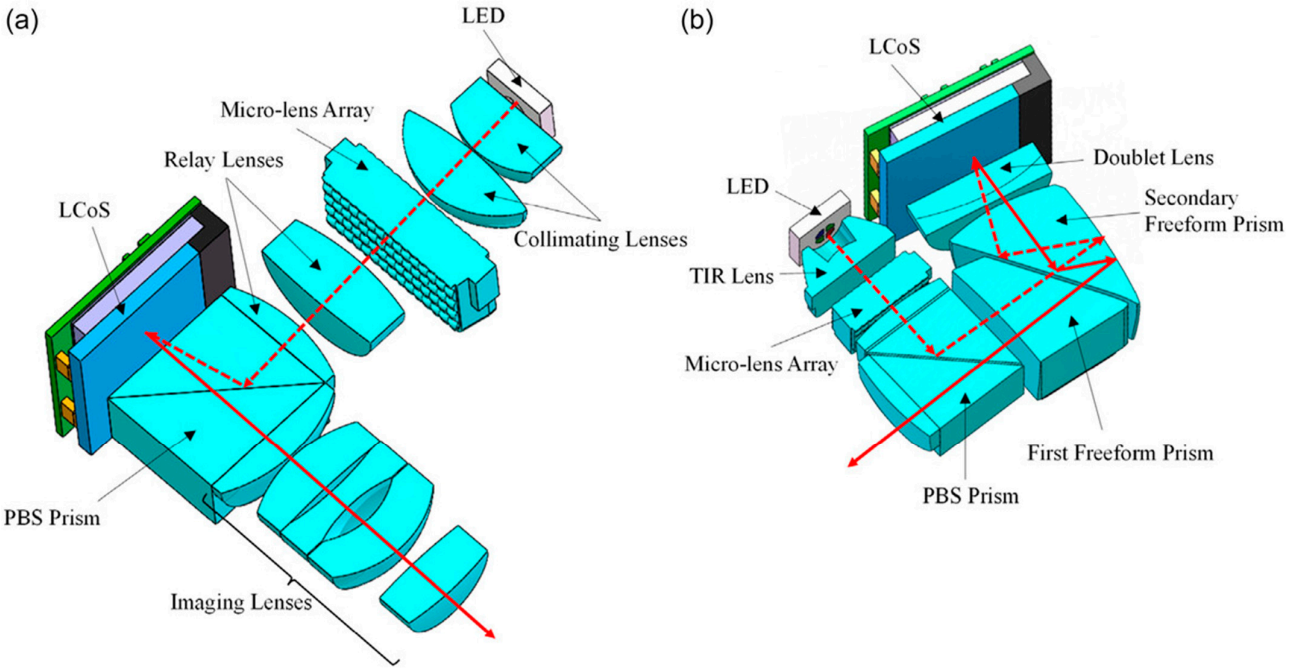

Figure 9. (**a**) Optical path diagram of previous design. (**b**) Optical path diagram of freeform projection optic design. From [170], originally published under a CC-BY license.

A very special application of freeform optics is eye implants [171]. Such an intraocular lens can, e.g., be used to overcome hyperopia or other misalignments of the human eye [172]. Accommodative intraocular lenses enable mimicking natural accommodation

by shifting the focus along the optical axis, with the Lumina Accommodative Intraocular Lens (AkkoLens International, Breda, The Netherlands) using an Alvarez system from two freeform lenses to achieve variable optics [173]. Another freeform intraocular lens is the Odyssey IOL, working with a freeform diffractive profile designed for the reduction of visual disturbances and chromatic aberration, which was already investigated in clinical studies [174,175]. Generally, besides simple intraocular lenses, freeform optics can be designed to optimize image contrast, focal range, and reduction of unwanted visual phenomena [176].

More often investigated are possibilities to use freeform optics in diverse cameras, e.g., compound-eye cameras or microscopic cameras [177]. For optical fiber endoscopes, the objective lens can be a freeform lens [178]. A tunable freeform lens system, based on the Alvarez principle, was used for an optical zoom endoscope with a zoom ratio of about 3 [179]. Correcting optical aberrations in order to enable full-color imaging was also achieved by an endoscope with multiple freeform surface lens elements [180]. Another application of small camera lenses is in miniaturization for mobile electronic devices, where freeform optics enable building wide-angle miniature lenses with small distortion and good image quality [181]. Especially for infrared cameras, where thermally induced defocusing is problematic, cubic freeform profiles can be used with an invariant focus across a region near the focal plane [112]. In space-based cameras, the required ultra-compact design is enabled by fully freeform cameras [182], while freeform microscope objectives can be applied for ultra-broadband microscopy [183].

4.3. Coupling and Structuring Optical Fiber Tips

Fiber-to-chip coupling is an important problem for the production of photonic integrated circuits [184]. This is why several research groups have investigated new methods to improve this coupling in terms of insertion losses, bandwidth density, sensitivity to misalignment, etc., many of them based on freeform optics. Using freeform reflective micro-optics, a new design approach was applied to simplify the high-dimensional freeform optimization problem to only two full-wave simulations, resulting in a low coupling loss around 0.5 dB at 1550 nm wavelength, combined with large alignment tolerance and high bandwidth density [185]. These values were also reached by the same research group working with micro-optical reflector arrays integrated with foundry-processed SiN photonics [186]. Another approach to designing freeform coupling elements included facet-attached beam-shaping elements [187,188].

It should be mentioned that there are diverse applications in sensing, imaging and optical trapping, working also with optical fibers, that necessitate structured tips of these optical fibers. Different freeform optics, such as dot-in-ring and ring-in-ring beam-shaping microlenses, have been fabricated on optical fiber tips, e.g., by two-photon polymerization [189]. Combinations of microlenses and connectors for photonic integrated circuits have also been reported, enabling, e.g., expanded beam coupling for higher alignment tolerances, hybrid integration of thick external components, mode size matching between edge couplers and single mode fibers, etc. [190].

4.4. Tunable/Actuated Freeform Micro-Optical Elements

Finally, we give some examples of tunable or actuated freeform micro-optical elements as well as the respective actuation mechanisms and discuss the importance of tunability for freeform micro-optics. Tuning the optical properties is possible, e.g., by modifying the refractive index distribution of a planar thermo-optical module by designed microheaters, which enables producing freeform optical wavefront modifications [191].

Actuated freeform elements can be moved, e.g., by magnetic actuation through ferromagnetic fluids that are injected into predefined microcavities, enabling actuation by external magnetic fields and removal by additional mechanical retracting elements [192]. Similarly, a bistable microlens actuator was discussed that could be switched between two stable positions using two coils around a polymeric micro-magnet [193]. Micro-coils were also used to stimulate endoscopic microsystems with embedded polymer-magnets, in this way enabling zooming as well as improved resolution and field of view [194]. Artificial muscles from a liquid-crystal elastomer were used to actuate an Alvarez lens system [195]. A dielectric elastomer actuator was used to prepare adaptive varifocal lenses with freeform surfaces [196]. Besides magnetic and electric stimuli, it is also possible to use photo-responsive materials for freeform optics, which enables controlling the optical properties of the devices by light [197].

While the recent literature does not give many examples of tunable freeform micro-optics, tunability is nevertheless highly important to further expand the applications of freeform optics. In this way, the phase, focal length, and intensity distribution can be dynamically controlled, enabling time-dependent optical properties beyond the static functionality [198]. Such reconfigurable freeform micro-optics can be used, e.g., in spaceborne remote sensing, active beam steering, or light-field displays [199].

As the aforementioned examples have already shown, different actuation mechanisms can be used for tunable freeform micro-optics. Micro-electromechanical systems (MEMS) enable very fast actuation of freeform optics with frequencies of several hundred kHz and response times in the microsecond range [200]. Electrostatic actuation, on the other hand, enables large tuning ranges on the millimeter scale, applying relatively low voltages, e.g., below 40 V [201]. Piezoelectric actuation offers even larger displacements, but needs longer response times and more energy [201]. Thermally actuated systems again have a lower power consumption and enable real-time modification of optical systems [202]. To combine the advantages of these different actuation mechanisms, electrostatic, piezoelectric, thermal and pneumatic systems are often combined [200].

Instead of changing the position of optical freeform elements, it is in principle also possible to modify the optical surfaces themselves. This, however, has more often been shown for conventional optofluidic lenses, probably due to the problematic stability and packaging of such optofluidic systems [203]. On the other hand, tunable metasurfaces, which can be regarded as planar freeform optics with nanostructures, can be tuned by the aforementioned mechanisms and can also contain liquid crystals, phase-change materials, and other materials that enable inherent changes in their optical properties [204], enabling new time-dependent functionalities [199]. Such metastructures can, e.g., be produced by different additive manufacturing techniques, as described in detail in Ref. [205].

As this discussion shows, there are several challenges for tunable freeform micro-optics. On the one hand, systems are usually either fast or enable larger deformations [200]. On the other hand, the reliability and cycle stability can be reduced by mechanical fatigue, thermal drift, or material degradation, depending on the used system [199]. Finally, precise alignment is also a problem for tunable freeform micro-optics, as well as for static systems [201].

Nevertheless, such tunable freeform micro-optics are highly interesting for diverse applications, such as imaging systems [201], non-imaging optics [198], photonic integrated circuits [206], or sensing and spectroscopy [202].

5. Opportunities and Challenges

Opportunities and challenges of freeform micro-optics are related to design, to manufacturing and metrology, to system integration and applications, and to the rapidly evolving field of research.

While removing the necessity of rotational symmetry by using freeform optics allows for building highly compact components with unprecedented optical performance, these advantages bring the problem of severely more complicated and less intuitive design of the optical components [8,207]. In addition, there is less experience in designing and optimizing freeform optics, as compared to conventional optics. This problem, however, may be coped with through a transition to artificial intelligence (AI)-driven design [208–211]. On the other hand, the large number of parameters that have to be calculated during freeform surface design necessitates high computational power and may lead to convergence difficulties during optimization [154]. It must also be mentioned that polarization effects, aberrations and other vectorial effects may lead to unexpected problems in strongly off-axis freeform systems, which have to be taken into account in design and optimization [211]. Besides these technical design problems, standardization and tolerancing frameworks are still missing, so reproducibility by other research groups is lower than for common optical elements, making the industrial adoption problematic [8].

Manufacturing of freeform optics is more complex than manufacturing of conventional optics. The absence of a symmetry axis necessitates sophisticated toolpath strategies and multi-axis machining to prepare accurate surface geometries and avoid tool interference [212]. On the other hand, subtractive manufacturing processes often have a trade-off between the necessary shape accuracy and the required low surface roughness [8]. In addition, measuring freeform surfaces poses new metrological challenges regarding stitching and data-processing [8]. It should be mentioned that not only the manufacturing itself, but also the potential difference between optimized designs and manufacturable geometries poses challenges for both design and manufacturing, making the implementation of design-for-manufacturing approaches necessary [8].

System integration is often improved by freeform optics that enable compact and lightweight optical systems in diverse applications [9,207]. Nevertheless, freeform optics have to be aligned very carefully, with a lower tolerance than conventional optics [8]. A very interesting upcoming area is the development of programmable and adaptive freeform optics; however, these are often limited by reduced efficiency and coherence restrictions [198].

In spite of the aforementioned challenges which still have to be overcome, freeform micro-optics enable new applications like compact imaging systems, wearable optics, optics for space applications, etc., where conventional optics reach their limits due to performance and size restrictions [8]. The research field of freeform micro-optics is rapidly growing to face the aforementioned challenges, which can be overcome by interdisciplinary research along the borders between design, manufacturing, and metrology [198].

6. Conclusions and Outlook

This review gives an overview of recent developments and limits in freeform micro-optical elements. While design and manufacturing have been significantly improved since the first approaches, all parts of the production chain can still be developed further. In particular, the use of affordable and widely available methods to produce freeform optics, e.g., by common 3D printing techniques such as SLA and DLP, should be further investigated.

As the sample applications mentioned here show, the use of freeform optics has developed from camera lenses towards miniaturized lenses for endoscopes or intraocular lenses, concentrators for solar panels and many more.

Future developments in freeform micro-optics can be based on more sophisticated design and manufacturing as well as the need for new applications. Design methodologies should take into account deterministic and inverse approaches as well as data-driven and AI-based design [208,210,213]. Combining the design of freeform micro-optical surfaces with mechanical structures and systems and other sophisticated design methods can further improve stability and reproducible alignment of highly integrated optical systems [39,214]. On the other hand, design-for-manufacturing approaches are necessary to build a bridge between theoretical optimization and manufacturability [8].

The extension of freeform optics for emerging applications, such as augmented/virtual reality or optics for space applications, is another important research area, where the aforementioned potential compactness of freeform micro-optics, as compared to conventional optics, offers advantages [215]. This goal can be accompanied by a reduction in optical elements to reduce the necessary alignment steps and the system complexity [214] as well as an increased use of reflective freeform optics to avoid problematic dispersion [216]. Besides the use of reflective optics, improved theoretical understanding of off-axis and non-symmetric aberrations has to be developed for complex freeform micro-optics [215]. Finally, new approaches combining freeform optics with digital post-processing, sometimes called computational optics, should be mentioned, which may enable creating high-performance optical systems [217].

Author Contributions: Conceptualization, T.B., G.E., J.F., R.K. and A.E.; methodology, T.B., R.K. and A.E.; formal analysis, A.E.; investigation, A.E.; resources, G.E.; writing—original draft preparation, A.E.; writing—review and editing, all authors; visualization, G.E. All authors have read and agreed to the published version of the manuscript.

Funding: This research received no external funding.

Institutional Review Board Statement: Not applicable.

Informed Consent Statement: Not applicable.

Data Availability Statement: No new data were created in this review.

Conflicts of Interest: The authors declare no conflicts of interest.

References

1. Fischer, R.E.; Tadic-Galeb, B.; Yoder, P.R. *Optical System Design*; McGraw-Hill: New York, NY, USA, 2008.
2. Voelkel, R. Micro-optics: Enabling technology for illumination shaping in optical lithography. *Proc. SPIE* **2014**, *9052*, 90521U.
3. Nicholas, D.J.; Boon, J.E. The generation of high precision aspherical surfaces in glass by CNC machining. *J. Phys. D. Appl. Phys.* **1981**, *14*, 593–600. [CrossRef]
4. Zhang, L.C.; Liu, W.D. Precision glass molding: Toward an optimal fabrication of optical lenses. *Front. Mech. Eng.* **2017**, *12*, 3–17. [CrossRef]
5. Blachowicz, T.; Ehrmann, G.; Ehrmann, A. Optical elements from 3D printed polymers. *e-Polymers* **2021**, *21*, 549–565. [CrossRef]
6. Blachowicz, T.; Ehrmann, A. 3D Printed MEMS Technology—Recent Developments and Applications. *Micromachines* **2020**, *11*, 434. [CrossRef] [PubMed]
7. Rolland, J.P.; Davies, M.A.; Suleski, T.J.; Evans, C.; Bauer, A.; Lambropoulos, J.C.; Falaggis, K. Freeform optics for imaging. *Optica* **2021**, *8*, 161–176. [CrossRef]
8. Kumar, S.; Tong, Z.; Jiang, X.Q. Advances in the design and manufacturing of novel freeform optics. *Int. J. Extrem. Manuf.* **2022**, *4*, 032004. [CrossRef]
9. Falaggis, K.; Rolland, J.; Duerr, F.; Sohn, A. Freeform optics: Introduction. *Opt. Express* **2022**, *30*, 6450–6455. [CrossRef]
10. González-Acuna, R.; Chaparro-Romo, H.A. The path of light. In *Optical Path Theory*; IOP Publishing Ltd.: Bristol, UK, 2022; pp. 1-1–1-27.
11. Malyshev, I.V.; Reunov, D.G.; Chkhalo, N.I.; Toropov, M.N.; Poestov, A.E.; Polkovnikov, V.N.; Tsybin, N.N.; Lopatin, A.Y.; Chernyshev, A.K.; Mikhailenko, M.S.; et al. High-aperture EUV microscope using multilayer mirrors and a 3D reconstruction algorithm based on z-tomography. *Opt. Express* **2022**, *30*, 47567–47586. [CrossRef]

12. Han, W.J.; Jeong, J.S.; Kim, J.S.; Kim, S.-J. Aberration Theory of a Flat, Aplanatic Metalens Doublet and the Design of a Meta-Microscope Objective Lens. *Sensors* **2023**, *23*, 9273. [CrossRef]
13. Yu, D.-X.; Jiang, Z.; Zheng, Y.; Zhang, H.-R.; Li, R.-Q.; Zhao, Y.-R.; Lu, X.-K.; Lin, Y.-C.; Liu, C.; Wang, Q.-H. Large zoom ratio and adaptive aberration correction microscope using 4DPSF-aware Physical Degradation-guided Network. *Light Sci. Appl.* **2026**, *15*, 140. [CrossRef] [PubMed]
14. Martinez, N. Atmospheric Pre-Compensation of Ground-to-Space Communications with Adaptive Optics: Past, Present and Future—A Field Review. *Photonics* **2023**, *10*, 858. [CrossRef]
15. Rao, C.H.; Zhong, L.B.; Guo, Y.M.; Li, M.; Zhang, L.Q.; Wei, K. Astronomical adaptive optics: A review. *PhotoniX* **2024**, *5*, 16. [CrossRef]
16. Fan, R.D.; Wang, Z.C.; Huang, L. Metasurfaces in Adaptive Optics: A New Opportunity in Optical Wavefront Sensing. *Laser Photonics Rev.* **2025**, *19*, e01566. [CrossRef]
17. Pozzi, P.; Quintavalla, M.; Wong, A.B.; Borst, J.G.G.; Bonora, S.; Verhaegen, M. Plug-and-play adaptive optics for commercial laser scanning fluorescence microscopes based on an adaptive lens. *Opt. Lett.* **2020**, *45*, 3585–3588. [CrossRef]
18. Furieri, T.; Ancora, D.; Calisesi, G.; Morara, S.; Bassi, A.; Bonora, S. Aberration measurement and correction on a large field of view in fluorescence microscopy. *Biomed. Opt. Express* **2021**, *13*, 262–273. [CrossRef]
19. Furieri, T.; Bassi, A.; Bonora, S. Large field of view aberrations correction with deformable lenses and multi conjugate adaptive optics. *J. Biophotonics* **2023**, *16*, e202300104. [CrossRef]
20. Ohland, J.B.; Lebas, N.; Deo, V.; Guyon, O.; Mathieu, F.; Audebert, P.; Papadopoulos, D. Apollon Real-Time Adaptive Optics: Astronomy-inspired wavefront stabilization in ultraintense lasers. *High Power Laser Sci. Eng.* **2025**, *13*, e29. [CrossRef]
21. Alvarez, L.W. Two-Element Variable-Power Spherical Lens. US Patent 3,305,294, 21 February 1967.
22. Lohmann, A.W. A new class of varifocal lenses. *Appl. Opt.* **1970**, *9*, 1669–1671. [CrossRef]
23. Barbero, S.; Rubinstein, J. Adjustable-focus lenses based on the Alvarez principle. *J. Opt.* **2011**, *13*, 125705. [CrossRef]
24. Bawart, M.; Jesacher, A.; Zelger, P.; Bernet, S.; Ritsch-Marte, M. Modified Alvarez lens for high-speed focusing. *Opt. Express* **2017**, *25*, 29847–29855. [CrossRef] [PubMed]
25. Aderneuer, T.; Fernández, O.; Chaves, J.; Mohedano, R.; Ferrini, R. Design for manufacturing tools for free-form micro-optical arrays. In *SPIE Proc. Optical Fabrication, Testing, and Metrology VII*; SPIE: Bellingham, WA, USA, 2021; Volume 11873, p. 1187304.
26. Ferrini, R. A new era for free-form micro-optics manufacturing: The final frontier. . .. In *OSA Optical Design and Fabrication 2021 (Flat Optics, Freeform, IODC, OFT)*; OSA Technical Digest, paper JTu3B.1; Capasso, F., Chen, W., Dainese, P., Fan, J., DeGroote Nelson, J., Duerr, F., Rogers, J., Rolland, J., Clark, P., Pfisterer, R., et al., Eds.; Optica Publishing Group: Washington, DC, USA, 2021.
27. Zanella, F.; Fernandez, O.; Offermans, T.; Aderneuer, T.; Chaves, J.; Mohedano, R.; Basset, G. Manufacturing acceleration of free-form micro-optical arrays (FMOAs) with CAD algorithms. In *SPIE Proc. Advanced Fabrication Technologies for Micro/Nano Optics and Photonics XVI*; SPIE: Bellingham, WA, USA, 2023; Volume 12433, p. 124330F.
28. Bösel, C.; Gross, H. Ray mapping approach for the efficient design of continuous freeform surfaces. *Opt. Express* **2016**, *24*, 14271–14282. [CrossRef] [PubMed]
29. Zhang, Y.; Wu, R.; Liu, P.; Zheng, Z.; Li, H.; Liu, X. Double freeform surfaces design for laser beam shaping with Monge-Ampère equation method. *Opt. Comm.* **2014**, *331*, 297–305. [CrossRef]
30. Brix, K.; Hafizogullari, Y.; Platen, A. Designing illumination lenses and mirrors by the numerical solution of Monge–Ampère equations. *J. Opt. Soc. Am. A* **2015**, *32*, 2227–2236. [CrossRef]
31. Wu, R.; Zhang, Y.; Sulman, M.M.; Zheng, Z.; Benítez, P.; Miñano, J.C. Initial design with L2 Monge-Kantorovich theory for the Monge-Ampère equation method in freeform surface illumination design. *Opt. Express* **2014**, *22*, 16161–16177. [CrossRef]
32. Oliker, V.I. Mathematical aspects of design of beam shaping surfaces in geometrical optics. In *Trends in Nonlinear Analysis*; Kirkilionis, M., Kromker, S., Rannacher, R., Tomi, F., Eds.; Springer: Berlin/Heidelberg, Germany, 2003; pp. 193–222.
33. Michaelis, D.; Schreiber, D.; Brauer, A. Cartesian oval representation of freeform optics in illumination systems. *Opt. Lett.* **2011**, *36*, 918–920. [CrossRef]
34. Schmidt, S.; Thiele, S.; Toulouse, A.; Bösel, C.; Tiess, T.; Herkommer, A.; Gross, H.; Giessen, H. Tailored micro-optical freeform holograms for integrated complex beam shaping. *Optica* **2020**, *7*, 1279–1286. [CrossRef]
35. Leiner, C.; Nemitz, W.; Schweitzer, S.; Wenzl, F.P.; Sommer, C. Design procedure for ultra-thin free-form micro-optical elements allowing for large DHR values and uniform irradiance distributions of ultrathin direct-lit luminaires. *OSA Contin.* **2020**, *3*, 3237–3252. [CrossRef]
36. Nie, Y.; Gross, H.; Zhong, Y.; Duerr, F. Freeform optical design for a nonscanning corneal imaging system with a convexly curved image. *Appl. Opt.* **2017**, *56*, 5630–5638. [CrossRef]
37. Wojtanowski, J.; Jakubaszek, M.; Zygmunt, M. Freeform mirror design for novel laser warning receivers and laser angle of incidence sensors. *Sensors* **2020**, *20*, 2569. [CrossRef]

38. Meng, Q.; Wang, H.; Wang, K.; Wang, Y.; Ji, Z.; Wang, D. Off-axis three-mirror freeform telescope with a large linear field of view based on an integration mirror. *Appl. Opt.* **2016**, *55*, 8962–8970. [CrossRef]
39. Xia, Y.; Huang, Y.W.; Yan, C.X.; Shao, M.X. Design Method of Freeform Surface Optical Systems with Low Coupling Position Error Sensitivity. *Sensors* **2024**, *24*, 4387. [CrossRef]
40. Novotny, L.; Beversluis, M.R.; Youngworth, K.S.; Brown, T.G. Longitudinal field modes probed by single molecules. *Phys. Rev. Lett.* **2001**, *86*, 5251–5254. [CrossRef]
41. D'Aguanno, G.; Mattiucci, N.; Bloemer, M.; Desyatnikov, A. Optical vortices during a superresolution process in a metamaterial. *Phys. Rev. A* **2008**, *77*, 043825. [CrossRef]
42. Kim, H.; Park, J.; Cho, S.-W.; Lee, S.-Y.; Kang, M.; Lee, B. Synthesis and dynamic switching of surface plasmon vortices with plasmonic vortex lens. *Nano Lett.* **2010**, *10*, 529–536. [CrossRef] [PubMed]
43. Boriskina, S.V.; Reinhard, B.M. Molding the flow of light on the nanoscale: From vortex nanogears to phase-operated plasmonic machinery. *Nanoscale* **2012**, *4*, 76–90. [CrossRef] [PubMed]
44. Nivas, J.J.; Cardano, F.; Song, Z.; Rubano, A.; Fittipaldi, R.; Vecchione, A.; Paparo, D.; Marrucci, L.; Bruzzese, R.; Amoruso, S. Surface structuring with polarization-singular femtosecond laser beams generated by a q-plate. *Sci. Rep.* **2017**, *7*, 42142. [CrossRef]
45. Piccirillo, B.; Picardi, M.F.; Marrucci, L.; Santamato, E. Flat polarization-controlled cylindrical lens based on the pancharatnam-berry geometric phase. *Eur. J. Phys.* **2017**, *38*, 034007. [CrossRef]
46. Jiang, M.; Yu, H.; Feng, X.; Guo, Y.; Chaganava, I.; Turiv, T.; Lavrentovich, O.D.; Wei, Q.H. Liquid crystal Pancharatnam-Berry micro-optical elements for laser beam shaping. *Adv. Opt. Mater.* **2018**, *6*, 1800961. [CrossRef]
47. Alemán-Castaneda, L.A.; Piccirillo, B.; Santamato, E.; Marrucci, L.; Alonso, M.A. Shearing interferometry via geometric phase. *Optica* **2019**, *6*, 396–399. [CrossRef]
48. Piccirillo, B.; Piedipalumbo, E.; Santamato, E. Geometric-Phase Waveplates for Free-Form Dark Hollow Beams. *Front. Phys.* **2020**, *8*, 94. [CrossRef]
49. Jahromi, H.S.; Kode, S.; Gilfoy, N.; Stepanova, T.; Menon, D. Enabling manufacturing of precision freeform glass optics using laser-assisted diamond turning. *Proc. SPIE* **2025**, *13728*, 137281K.
50. You, K.Y.; Liu, G.Y.; Wang, W.; Fang, F.Z. Laser assisted diamond turning of silicon freeform surface. *J. Mater. Process. Technol.* **2023**, *322*, 118172. [CrossRef]
51. Zhang, L.; Sato, Y.; Yan, J. Optimization of fast tool servo diamond turning for enhancing geometrical accuracy and surface quality of freeform optics. *J. Adv. Mech. Des. Syst. Manuf.* **2023**, *17*, 22–00227. [CrossRef]
52. Zhang, X.Q.; Wu, H.; Yu, Y.Q.; Jia, Z.L.; Wang, X.Y.; Ren, M.J.; Zhu, L.M. Model-free tool path modification in ultra-precision diamond turning of freeform surfaces using iterative learning control. *Prec. Eng.* **2025**, *94*, 736–748. [CrossRef]
53. Prasad, K.K.; Singh, M.P.; Negi, V.S.; Mishra, V.; Jha, S.; Khan, G.S. Ductile machining of single-crystal germanium freeform optics via ultra-precision diamond turning for high-performance infrared imaging systems. *Precis. Eng.* **2025**, *96*, 380–397. [CrossRef]
54. Hashimoto, T.; Yan, J.W. Time delay compensation in high-speed diamond turning of freeform surface using independent fast tool servo with a long stroke. *Prec. Eng.* **2025**, *93*, 515–527. [CrossRef]
55. Guo, P.; Wei, Z.P.; Zhang, S.J.; Xiong, Z.W.; Liu, M.Y. Feature-adaptive toolpath planning with enhanced surface texture uniformity for ultra-precision diamond milling of freeform optics. *J. Mater. Process. Technol.* **2024**, *323*, 118220. [CrossRef]
56. Wu, P.Y.; Guo, P.; Xiong, Z.W.; Dong, Z.W.; Zhang, S.J. Multi-technique based coarse to fine form registration for ultra-precision diamond milling of freeform optics. *Meas. Sci. Technol.* **2025**, *36*, 015016. [CrossRef]
57. Li, P.Z.; Wang, S.J.; To, S.; Sun, Z.W.; Jiao, J.; Xu, S.J. High-efficient fabrication of infrared optics with uniform microstructures by a semi-ductile diamond milling approach. *Int. J. Adv. Manuf. Technol.* **2023**, *126*, 919–934. [CrossRef]
58. Sun, Z.W.; To, S.; Wang, S.J. Diamond Milling System for Fabricating Infrared Micro-optics Arrays. In *Fabrication of Micro/Nano Structures via Precision Machining*; Zhang, G., Xu, B., Lu, Y., To, S., Eds.; Springer: Singapore, 2023; pp. 103–128.
59. Huang, C.A.; Yang, S.W.; Shen, C.H.; Cheng, K.C.; Wang, H.; Lai, P.L. Fabrication and evaluation of electroplated Ni–diamond and Ni–B–diamond milling tools with a high density of diamond particles. *Int. J. Adv. Manuf. Technol.* **2019**, *104*, 2981–2989. [CrossRef]
60. Tian, C.C.; Chen, C.; Wan, Y.; Li, X.K. Research Progress on Additively Manufactured Diamond Tools. *Materials* **2025**, *18*, 5540. [CrossRef] [PubMed]
61. Song, J.C.; Tong, Z.; Yao, Z.Y.; Jiang, X.Q. Micro milling of fused silica using picosecond laser shaped single crystal diamond tools. *Front. Mater.* **2023**, *10*, 1176545. [CrossRef]
62. Kong, L.B.; Cheung, C.F. Integrated Manufacturing of Ultra-precision Freeform Optics. In *Precision Machining Process and Technology*; Yang, S., Ed.; Springer Nature: Singapore, 2024; pp. 1–27.
63. Zhang, C.P.; Sun, J.Z.; Zhou, J.; Chen, X. Design and Study of Machine Tools for the Fly-Cutting of Ceramic-Copper Substrates. *Materials* **2024**, *17*, 1111. [CrossRef]
64. Zhang, G.Q.; Zhang, X.; Ma, S.; Luo, T.; Cao, S.K.; Wang, J.P.; Ma, Y.T.; Jiang, J.K.; Wang, H.T. Tool path modeling and fabrication of multi-boundary lens array by tool offset end-fly-cutting. *J. Manufact. Process.* **2023**, *85*, 356–367. [CrossRef]

65. Bu, Y.B.; Chen, Y.; Min, Q.; Zhang, C.X.; Qing, J.B. Three-dimensional modeling and experimental analysis of diamond fly-cutting for anti-reflective microgroove arrays on BK7 glass. *Int. J. Adv. Manufact. Technol.* **2025**, *139*, 6307–6323. [CrossRef]
66. Wang, J.P.; Zhang, G.P.; Jiang, J.K. Tool Offset Flycutting Straight-Groove-Type Microstructures. In *Fabrication of Micro/Nano Structures via Precision Machining*; Zhang, G., Xu, B., Lu, Y., To, S., Eds.; Springer: Singapore, 2023; pp. 15–39.
67. Wang, S.; Zhao, Q.L. Development of an on-machine measurement system with chromatic confocal probe for measuring the profile error of off-axis biconical free-form optics in ultra-precision grinding. *Measurement* **2022**, *202*, 111825. [CrossRef]
68. Wang, S.; Zhao, Q.L.; Guo, B. Ultra-precision Ductile Grinding of Off-Axis Biconical Free-Form Optics with a Controllable Scallop Height Based on Slow Tool Servo with Diamond Grinding Wheels. *Int. J. Precis. Eng. Manuf.—Green. Tech.* **2023**, *10*, 1169–1188. [CrossRef]
69. Procháska, F.; Tomka, D.; Vavruska, P.; Paprcková, M.; Melich, R.; Matousek, O.; Lhomé, E. Innovative process for precise grinding of optical free-form elements. *J. Instrum.* **2023**, *18*, P04022. [CrossRef]
70. Peng, L.R.; Li, X.C.; Li, L.Z.; Cheng, Q.; Luo, X.; Zhou, X.Q.; Zhang, X.J. Application of the Improved Grinding Technology to Freeform Surface Manufacturing. *Photonics* **2023**, *10*, 240. [CrossRef]
71. Müller, H.; Henkel, S.; Schulze, C.; Frank, S.; Bliedtner, J.; Arnold, T. Freeform surfaces manufactured with a combination of ultra-fine grinding and plasma jet polishing. *J. Eur. Opt. Soc.—Rapid Publ.* **2025**, *21*, 12. [CrossRef]
72. Böttger, G.; Link, S.; Gomez, C.; Weissenburg, L.F.; Schröder, H.; Schneider-Ramelow, M. Versatile micro-optical coupling platform created by selective laser etching and smoothing of thin glass. *Proc. SPIE* **2025**, *13372*, 1337207.
73. Van Gorp, T.; Benoit, A.; Ross, C.A.; Roldán-Varona, P.; Evans, C.; Lee, D.; Hand, D.P.; Thomson, R.R. Towards freeform reflective fused silica optics using ultrafast laser-assisted etching. *Proc. SPIE* **2024**, *13100*, 131007A.
74. Yu, J.P.; Xu, J.; Huang, J.X.; Chen, J.F.; Qi, J.; Cheng, Y. Single-mode bending optofluidic waveguides and beam splitters in fused silica enabled by polarization-independent femtosecond-laser-assisted etching. *Photonics Res.* **2025**, *13*, 1562–1571. [CrossRef]
75. Hua, J.-G.; Liang, S.-Y.; Chen, Q.-D.; Juodkazis, S.; Sun, H.-B. Free-Form Micro-Optics Out of Crystals: Femtosecond Laser 3D Sculpturing. *Adv. Funct. Mater.* **2022**, *32*, 2200255. [CrossRef]
76. Hua, J.-G.; Ren, H.; Huang, J.T.; Luan, M.-L.; Chen, Q.-D.; Juodkazis, S.; Sun, H.-B. Laser-Induced Cavitation-Assisted True 3D Nano-Sculpturing of Hard Materials. *Small* **2023**, *19*, 2207968. [CrossRef] [PubMed]
77. Xu, S.; Fan, H.; Xu, S.-J.; Li, Z.-Z.; Lei, Y.H.; Wang, L.; Song, J.-F. High-Efficiency Fabrication of Geometric Phase Elements by Femtosecond-Laser Direct Writing. *Nanomaterials* **2020**, *10*, 1737. [CrossRef]
78. Zubauskas, L.; Markauskas, E.; Vysniauskas, A.; Stankevic, V.; Gecys, P. Comparative analysis of microlens array formation in fused silica glass by laser: Femtosecond versus picosecond pulses. *J. Sci. Adv. Mater. Dev.* **2024**, *9*, 100804. [CrossRef]
79. Kong, D.J.; Wang, G.L.; Zhang, L.M.; Chen, S.T.; Sun, X.Y.; Hu, Y.W.; Duan, J.A. Formation of 3D Free-Form Artificial Compound Eye Mold by Maskless Discrete Wet-Etching on Flat Fused Silica. *Adv. Opt. Mater.* **2025**, *13*, e02163. [CrossRef]
80. Skora, J.L.; Gaiffe, O.; Bargiel, S.; Tavernier, L.; de Labachelerie, M.; Passilly, N. Micro-Optical Components Manufactured in Glass by Femtosecond Laser Irradiation Followed by Chemical Etching. In Proceedings of the International Symposium on Optomechatronic Technology (ISOT 2021), Besançon, France, 2–5 November 2021.
81. Zhou, W.J.; Li, R.; Li, M.; Tao, P.; Wang, X.S.; Dai, S.X.; Song, B.A.; Zhang, W.; Lin, C.G.; Shen, X.; et al. Fabrication of microlens array on chalcogenide glass by wet etching-assisted femtosecond laser direct writing. *Ceram. Int.* **2022**, *48*, 18983–18988. [CrossRef]
82. Zhan, Q.S.; He, S.P.; Wen, Z.C.; Yan, M.F.; Zou, Q.S.; Zhang, W.; Song, B.A.; Dai, S.X.; Zhang, P.Q. Preparation of microlens arrays on tellurite glass via wet etching assisted by femtosecond laser direct writing. *Opt. Laser Technol.* **2025**, *189*, 113117. [CrossRef]
83. Sharma, E.; Rathi, R.; Misharwal, J.; Sinhmar, B.; Kumari, S.; Dalal, J.; Kumar, A. Evolution in Lithography Techniques: Microlithography to Nanolithography. *Nanomaterials* **2022**, *12*, 2754. [CrossRef]
84. Skliutas, E.; Merkininkaité, G.; Maruo, S.; Zhang, W.X.; Chen, W.Y.; Deng, W.T.; Greer, J.; von Freymann, G.; Malinauskas, M. Multiphoton 3D lithography. *Nat. Rev. Methods Primers* **2025**, *5*, 15. [CrossRef]
85. Gonzalez-Hernandez, D.; Varapnickas, S.; Bertoncini, A.; Liberale, C.; Malinauskas, M. Micro-Optics 3D Printed via Multi-Photon Laser Lithography. *Adv. Opt. Mater.* **2023**, *11*, 2201701. [CrossRef]
86. Varapnickas, S.; Thodika, S.C.; Moroté, F.; Juodkazis, S.; Malinauskas, M.; Brasselet, E. Birefringent optical retarders from laser 3D-printed dielectric metasurfaces. *Appl. Phys. Lett.* **2021**, *118*, 151104. [CrossRef]
87. Lamprecht, B.; Ulm, A.; Lichtenegger, P.; Leiner, C.; Nemitz, W.; Sommer, C. Origination of free-form micro-optical elements using one- and two-photon grayscale laser lithography. *Appl. Opt.* **2022**, *61*, 1863–1875. [CrossRef]
88. Aderneuer, T.; Fernández, O.; Ferrini, R. Two-photon grayscale lithography for free-form micro-optical arrays. *Opt. Express* **2021**, *29*, 39511–39520. [CrossRef]
89. Weinacker, J.; Kalt, S.; Kiefer, P.; Rietz, P.; Wegener, M. On Iterative Pre-Compensation of 3D Laser-Printed Micro-Optical Components Using Confocal-Optical Microscopy. *Adv. Funct. Mater.* **2024**, *34*, 2309356. [CrossRef]
90. Lutey, A.H.A.; Kuhness, D.; Mckee, S.; Ferraro, V.; Negozio, M.; Belardi, W.; Romoli, L.; Postl, M.; Stadlober, B. Data-driven optimization of maskless grayscale laser lithography. *Sci. Rep.* **2025**, *15*, 40063. [CrossRef]

91. Hafttananian, M.; Neild, A.; Cadarso, V.J. Integratable micro-optical compound objective lens using soft lithography. *Sens. Actuators A Phys.* **2023**, *360*, 114512. [CrossRef]
92. Xu, J.J.; Harasek, M.; Gföhler, M. From Soft Lithography to 3D Printing: Current Status and Future of Microfluidic Device Fabrication. *Polymers* **2025**, *17*, 455. [CrossRef]
93. Galvanauskas, K.; Zvirblis, R.; Balcas, G.; Gailevicius, D.; Astrauskyte, D.; Grineviciute, L.; Malinauskas, M. High-transparency and heavy-durability 3D micro-optics made via ultrafast laser lithography combined with atomic layer deposition and calcination. In *Proceedings of Conference on Lasers and Electro-Optics/Europe (CLEO/Europe 2023) and European Quantum Electronics Conference (EQEC 2023)*; Technical Digest Series, paper ce_11_2; Optica Publishing Group: Washington, DC, USA, 2023.
94. Astrauskyte, D.; Galvanauskas, K.; Gailevicius, D.; Drazdys, M.; Malinauskas, M.; Grineviciute, L. Deposition of thin films on hybrid-polymer 3D micro-optics using atomic layer deposition. *Proc. SPIE* **2024**, *13020*, 1302002.
95. Toombs, J.T.; Luitz, M.; Cook, C.C.; Jenne, S.; Li, C.C.; Rapp, B.E.; Kotz-Helmer, F.; Taylor, H.K. Volumetric additive manufacturing of silica glass with microscale computed axial lithography. *Science* **2022**, *376*, 308–312. [CrossRef] [PubMed]
96. Ocier, C.R.; Richards, C.A.; Bacon-Brown, D.A.; Ding, Q.; Kumar, R.; Garcia, T.J.; van de Groep, J.; Song, J.-H.; Cyphersmith, A.J.; Rhode, A.; et al. Direct laser writing of volumetric gradient index lenses and waveguides. *Light Sci. Appl.* **2020**, *9*, 196. [CrossRef] [PubMed]
97. Farsari, M. Advances in 3D and 4D multi-photon printing for micro and nano photonics [Invited]. *Opt. Mater. Express* **2025**, *15*, 2770–2791. [CrossRef]
98. Wang, H.; Zhang, W.; Ladika, D.; Yu, H.Y.; Gailevicius, D.; Wang, H.T.; Pan, C.-F.; Nair, P.N.S.; Ke, Y.J.; Mori, T.; et al. Two-Photon Polymerization Lithography for Optics and Photonics: Fundamentals, Materials, Technologies, and Applications. *Adv. Funct. Mater.* **2023**, *33*, 2214211. [CrossRef]
99. El-Tamer, A.; Surnina, M.; Hinze, U.; Chichkov, B.N. 3D Micro- and Nanostructuring by Two-Photon Polymerization. In *High Resolution Manufacturing from 2D to 3D/4D Printing*; Marasso, S.L., Cocuzza, M., Eds.; Springer: Cham, Switzerland, 2022; pp. 47–79.
100. Balcas, G.; Malinauskas, M.; Farsari, M.; Juodkazis, S. Fabrication of Glass-Ceramic 3D Micro-Optics by Combining Laser Lithography and Calcination. *Adv. Funct. Mater.* **2023**, *33*, 2215230. [CrossRef]
101. Plank, H.; Gspan, C.; Dienstleder, M.; Kothleitner, G.; Hofer, F. The influence of beam defocus on volume growth rates for electron beam induced platinum deposition. *Nanotechnology* **2008**, *19*, 485302. [CrossRef]
102. Huang, P.-H.; Laakso, M.; Edinger, P.; Hartwig, O.; Duesberg, G.S.; Lai, L.-L.; Mayer, J.; Nyman, J.; Errando-Herranz, C.; Stemme, G.; et al. Three-dimensional printing of silica glass with sub-micrometer resolution. *Nat. Comm.* **2023**, *14*, 3305. [CrossRef]
103. Gonzalez-Utrera, D.; Villalobos-Mendoza, B.; Diaz-Uribe, R.; Aguirre-Aguirre, D. Modeling, fabrication, and metrology of 3D printed Alvarez lenses prototypes. *Opt. Express* **2024**, *32*, 3512–3527. [CrossRef]
104. Nair S, P.; Wang, H.T.; Trisno, J.; Ruan, Q.F.; Rezaei, S.D.; Simpson, R.E.; Yang, J.K.W. 3D Printing Mesoscale Optical Components with a Low-Cost Resin Printer Integrated with a Fiber-Optic Taper. *ACS Photonics* **2022**, *9*, 2024–2031. [CrossRef]
105. Webber, D.; Zhang, Y.J.; Sampson, K.L.; Picard, M.; Lacelle, T.; Paquet, C.; Boisvert, J.; Orth, A. Micro-optics fabrication using blurred tomography. *Optica* **2024**, *11*, 665–672. [CrossRef]
106. Beckert, E. 3D Printing of Optics. In *Inkjet Printing in Industry*; Zapka, W., Ed.; Wiley-VCH GmbH: Weinheim, Germany, 2022; pp. 1403–1416.
107. Williams, G.M.; Harmon, J.P. Additive manufacturing of gradient index optics. *Proc. SPIE* **2024**, *12798*, 1279820.
108. Williams, G.M.; Lunin, M.; Harmon, J.P. Advancing freeform gradient index (GRIN) optics for vision correction. *Proc. SPIE* **2025**, *13466*, 134660F.
109. Sieber, I.; Thelen, R.; Gengenbach, U. Enhancement of High-Resolution 3D Inkjet-Printing of Optical Freeform Surfaces Using Digital Twins. *Micromachines* **2021**, *12*, 35. [CrossRef]
110. Assefa, B.G.; Pekkarinen, M.; Parnanen, H.; Biskop, J.; Turunen, J.; Saarinen, J. Imaging-quality 3D-printed centimeter-scale lens. *Opt. Express* **2019**, *27*, 12630–12637. [CrossRef]
111. Den, Y.M.; Guo, X.G.; Kang, R.K.; Gao, S. Multi-factor and multi-scale material removal function modeling and experimental validation for bonnet polishing of freeform optical elements. *Tribol. Int.* **2025**, *210*, 110757.
112. Pant, L.M.; Sing, M.P.; Chandra, K.; Mishra, V.; Pandey, N.; Pant, K.K.; Khan, G.S.; Sakher, C. Development of cubic freeform optical surface for wavefront coding application for extended depth of field Infrared camera. *Infrared Phys. Technol.* **2022**, *127*, 104377. [CrossRef]
113. Peng, L.R.; Wang, Y.R.; Chen, H.; Li, L.X.; Cheng, Q.; Zhou, X.Q.; Zhang, X.J. Cross-scale surface shape error correction in the bonnet polishing of a freeform surface. *Appl. Opt.* **2024**, *63*, 6786–6793. [CrossRef]
114. Rajput, A.S.; Das, M.; Kapil, S. Investigations on a hybrid chemo-magnetorheological finishing process for freeform surface quality enhancement. *J. Manuf. Process.* **2022**, *81*, 522–536. [CrossRef]
115. Wang, B.; Tie, G.P.; Shi, F.; Zhang, W.L.; Song, C.; Guo, S.P. Design and frequency control study of small-sized magnetorheological finishing device applied in optical manufacturing. *J. Manuf. Process.* **2023**, *108*, 863–876. [CrossRef]

116. Raza, M.; Alam, Z.; Udai, A.D. Robot-assisted magnetorheological finishing of freeform surfaces using industrial 3-D camera. *Mater. Manuf. Process.* **2025**, *40*, 1094–1103. [CrossRef]
117. Muecke, D.; Jenne, S.; Esen, C.; Hellmann, R. Hybrid laser fabrication of LED beam-shaping optics in fused silica: Role of laser polishing. *Proc. SPIE* **2026**, *13881*, 138810I.
118. Porwol, T.; Kinast, J.; Cai, L.; Steinkopf, R.; Risse, S. Super-polished metallic freeform optics for EUV-application. *Proc. SPIE* **2024**, *12953*, 1295318.
119. Kahle, M.; Conrad, D.; Fricke, S.; Wilkens, L. Direct, Laser-based Production of Optics. *JLMN—J. Laser Micro/Nanoeng.* **2022**, *17*, 156–161.
120. Yadav, H.N.S.; Kumar, M.; Kumar, A.; Das, M. Plasma polishing processes applied on optical materials: A review. *J. Micromanufact.* **2023**, *6*, 27–39. [CrossRef]
121. Fan, Z.; Li, Z.L.; Wang, R.; Yu, N.; Ren, M.J.; Zhang, X.Q.; Zhu, L.M. A novel and efficient multi-jet plasma polishing process for optical fabrication. *J. Mater. Process. Technol.* **2025**, *337*, 118735. [CrossRef]
122. Arnold, T.; Boehm, G.; Mueller, H.; Ehrhardt, M.; Zimmer, K. Plasma jet assisted polishing of fused silica freeform optics. *EPJ Web Conf.* **2022**, *266*, 03001. [CrossRef]
123. Yadav, H.N.S.; Gupta, V.; Das, M. Numerical simulation and experimental investigation of novel developed medium-pressure plasma polishing process of fused silica. *Ceram. Int.* **2025**, *51*, 12691–12710. [CrossRef]
124. Xie, M.L.; Pan, Y.P.; An, Z.J.; Huang, S.J.; Dong, M. Review on Surface Polishing Methods of Optical Parts. *Adv. Mater. Sci. Eng.* **2022**, *2022*, 8723269. [CrossRef]
125. Liu, S.K.; Cheng, K. Cutting forces in ultraprecision machining freeform optics: Analysis through virtual simulations and experiments. *Sci. Talks* **2024**, *12*, 100392. [CrossRef]
126. Sun, L.H.; Chen, M.H.; He, T.; Yan, H.Z.; To, S.; Wu, Y.B.; Yip, W.S. Enhancing ductile regime ultra-precision diamond turning of curved zinc selenide (ZnSe) optics by using straight-nosed diamond tools with cutting-edge-slipping. *J. Manufact. Proc.* **2024**, *120*, 234–249. [CrossRef]
127. Sato, Y.; Yan, J.W. Tool path generation and optimization for freeform surface diamond turning based on an independently controlled fast tool servo. *Int. J. Extrem. Manuf.* **2022**, *4*, 025102. [CrossRef]
128. Kumar, S.; Zhong, W.B.; Yu, G.Y.; Zhang, J.F.; Zeng, W.H.; Jiang, X.Q. Investigation of surface imperfection in freeform optics with high-order XY polynomial design. *Int. J. Adv. Manuf. Technol.* **2024**, *130*, 1735–1747. [CrossRef]
129. Wang, D.F.; Sui, Y.X.; Yang, H.J.; Li, D. Adaptive Spiral Tool Path Generation for Diamond Turning of Large Aperture Freeform Optics. *Materials* **2019**, *12*, 810. [CrossRef] [PubMed]
130. Butkutė, A.; Merkininkaitė, G.; Jurksas, T.; Stancikas, J.; Baravykas, T.; Vargalis, R.; Tickunas, T.; Bachmann, J.; Sakirzanovas, S.; Jonusauskas, L. Femtosecond Laser Assisted 3D Etching Using Inorganic-Organic Etchant. *Materials* **2022**, *15*, 2817. [CrossRef]
131. Song, Y.P.; Xu, J.; Liu, Z.X.; Zhang, A.D.; Yu, J.P.; Qi, J.; Chen, W.; Cheng, Y. Fabrication of high-aspect-ratio fused silica microstructures with large depths using Bessel-beam femtosecond laser-assisted etching. *Opt. Laser Technol.* **2024**, *170*, 110305. [CrossRef]
132. Wang, B.-X.; Qi, J.-Y.; Lu, Y.-M.; Zheng, J.-X.; Xu, Y.; Liu, X.-Q. Rapid Fabrication of Smooth Micro-Optical Components on Glass by Etching-Assisted Femtosecond Laser Modification. *Materials* **2022**, *15*, 678. [CrossRef]
133. Kratz, M.; Kniffler, M.; Häfner, C.L. Influence of flexible multibeam intensity distributions on selective laser-induced etching process regimes. *Opt. Express* **2024**, *32*, 36453–36468. [CrossRef]
134. Siegle, L.; Ristok, S.; Giessen, H. Complex aspherical singlet and doublet microoptics by grayscale 3D printing. *Opt. Express* **2023**, *31*, 4179–4189. [CrossRef]
135. Zhu, D.X.; Zhang, J.; Xu, Q.; Li, Y.G. Two-photon polymerization of silica glass diffractive micro-optics with minimal lateral shrinkage. *Opt. Express* **2023**, *31*, 36037–36047. [CrossRef]
136. Duan, Y.T.; Zhang, X.D. Freeform optics characterization with surface registration and fitting algorithms for optical point-based spatial path 3D topography metrology. *Appl. Opt.* **2023**, *62*, 573–583. [CrossRef] [PubMed]
137. Guerra, M.G.; Lavecchia, F. Measurement of additively manufactured freeform artefacts: The influence of surface texture on measurements carried out with optical techniques. *Measurement* **2023**, *209*, 112540. [CrossRef]
138. Zhang, X.; Hu, H.X.; Xue, D.L.; Cheng, Q.; Yang, X.; Tang, W.; Qiao, G.B.; Zhang, X.J. Wavefront optical spacing of freeform surfaces and its measurement using CGH interferometry. *Opt. Laser Eng.* **2023**, *161*, 107350. [CrossRef]
139. Lyu, H.Y.; Kong, L.B.; Wang, S.X.; Xu, M. Robust and accurate measurement of optical freeform surfaces with wavefront deformation correction. *Opt. Express* **2022**, *30*, 7831–7844. [CrossRef]
140. Jiang, S.Y.; He, Q.Z.; Xing, Y.F.; Liu, L.X.; Yang, J.M. Multi-view stitching phase measuring deflectometry for freeform specular surface metrology. *Opt. Express* **2023**, *31*, 36557–36567. [CrossRef]
141. Wang, J.; Wang, X.K.; Peng, L.R.; Wang, J.C.; Liu, Z.K.; Li, L.Z.; Cai, M.X.; Liu, B.; Li, W.H.; Zhang, X.J. Method for testing freeform surfaces based on a Shack-Hartmann sensor with plane wavefront scanning and stitching. *Opt. Express* **2023**, *31*, 36702–36724. [CrossRef]

142. Ma, X.X.; Wang, J.L.; Wang, B.; Liu, X.Y.; Chen, Y.J. Research on Optical Metrology for Complex Optical Surfaces with Focal Plane Wavefront Sensing. *Micromachines* **2023**, *14*, 1142. [CrossRef]
143. Fan, R.D.; Wei, S.L.; Ji, H.R.; Qian, Z.; Tan, H.; Mo, Y.; Ma, D.L. Surface variation analysis of freeform optical systems over surface frequency bands for prescribed wavefront errors. *Opt. Laser Technol.* **2024**, *178*, 111223. [CrossRef]
144. Shahinian, H.; Hovis, C.D.; Evans, C.J. Effect of retrace error on stitching coherent scanning interferometry measurements of freeform optics. *Opt. Express* **2021**, *29*, 28562–28573. [CrossRef]
145. Liu, Y.L.; Dai, Y.J.; Shen, F.Q.; Yang, L.; Ding, Z.H.; Zheng, Z.R.; Wu, R.M.; Xu, L. High-performance imaging with an advanced non-imaging lens based on full-path optical diffraction calculation in two-dimensional space. *Opt. Express* **2022**, *30*, 11014–11025. [CrossRef]
146. Sun, H.L.; Li, S.J.; Feng, D.W.; Ni, Y.J.; Yu, S.F.; Song, J.K.; Ren, B.Q.; Ma, D.L.; Duan, M.F.; Lin, B.R. Advancing fiber-optic daylighting system integrated with freeform optics for indoor workstation lighting. *Build. Simul.* **2025**, *18*, 2923–2944. [CrossRef]
147. Wei, S.L.; Zhu, Z.B.; Ma, D.L. Efficient and compact freeform optics design for customized LED lighting. *Opt. Laser Technol.* **2023**, *167*, 109775. [CrossRef]
148. Meuret, Y.; Cerpentier, J. Design of freeform LED illumination lenses without glare. *Proc. SPIE* **2025**, *13597*, 135970B.
149. Meng, X.-I.; Ren, F.-P.; Zhang, P.; Tang, Z.-X. Trough-Type Free-Form Secondary Solar Concentrator for CPV/T Application. *Energies* **2022**, *15*, 8023. [CrossRef]
150. Zhu, Z.B.; Yang, L.; Ma, D.L. Freeform mirror array design for concentrating sunlight onto a CPV solar cell. *Appl. Opt.* **2023**, *62*, 3822–3828. [CrossRef]
151. Jost, N.; Jacobo-Martín, A.; Vallerotto, G.; Hernández, J.J.; Garcia-Sanchez, A.; Domínguez, C.; Rodríguez, I.; Antón, I. Fabrication of high-performance lens arrays for micro-concentrator photovoltaics using ultraviolet imprinting. *Int. J. Adv. Manuf. Technol.* **2024**, *131*, 5961–5970. [CrossRef]
152. Liu, J.N.; Jiang, P.; Yang, H.J.; Wang, D.Y. A beam shaping and collimation technique using freeform optics optimized by NSGA-II. *Opt. Commun.* **2025**, *596*, 132411. [CrossRef]
153. Li, Z.R.; Li, B.H.; Liu, D.J.; Jing, L.Q.; Wang, J.Q.; Fu, C.L.; Wang, Y.P.; Liao, C.R. Doughnut beam shaping based on a 3D nanoprinted microlens on fiber tip. *Opt. Laser Technol.* **2023**, *167*, 109798. [CrossRef]
154. Madrid-Sánchez, A.; Duerr, F.; Nie, Y.F.; Thienpont, H.; Ottevaere, H. Freeform optics design method for illumination and laser beam shaping enabled by least squares and surface optimization. *Optik* **2022**, *269*, 169941. [CrossRef]
155. Cai, Y.X.; Li, M.M.; Yi, A.Y.; Chen, S.-C.; Feng, Z.X.; Liu, X.H. A high-throughput framework from design to fabrication of freeform diffractive optical elements for beam shaping. *Opt. Laser Technol.* **2025**, *192*, 113724. [CrossRef]
156. Cerpentier, J.; Meuret, Y. Real-time, broadband beam shaping with programmable freeform topologies. *J. Phys. Photonics* **2026**, *8*, 015021. [CrossRef]
157. Yu, S.L.; Lu, J.S.; Ginis, V.; Kheifets, S.; Lim, S.W.D.; Qiu, M.; Gu, T.; Hu, J.J.; Capasso, F. On-chip optical tweezers based on freeform optics. *Optica* **2021**, *8*, 409–414. [CrossRef]
158. Beaucamp, A. Automated design of freeform optical systems by reverse ray-tracing and AI. *Proc. SPIE* **2025**, *13601*, 1360104.
159. Le Priol, E.; Sasaki, A.; Beaucamp, A. Light-field based 3D optical tweezers. *EPJ Web Conf.* **2024**, *309*, 10004. [CrossRef]
160. De Coster, D.; Loterie, D.; Ottevaere, H.; Vervaeke, M.; van Erps, J.; Missinne, J. Free-Form Optics Enhanced Confocal Raman Spectroscopy for Optofluidic Lab-on-Chips. *IEEE J. Sel. Top. Quantum Electron.* **2015**, *21*, 79–86. [CrossRef]
161. Grabe, T.; Li, Y.; Krauss, H.; Wolf, A.; Wu, J.J.; Yao, C.Y.; Wang, Q.; Lachmayer, R.; Ren, W. Freeform optics design for Raman spectroscopy. *Proc. SPIE* **2020**, *11287*, 112870A.
162. Hua, J.-G.; Ren, H.; Jia, A.; Tian, Z.-N.; Wang, L.; Juodkazis, S.; Chen, Q.-D.; Sun, H.-B. Convex silica microlens arrays via femtosecond laser writing. *Opt. Lett.* **2020**, *45*, 636–639. [CrossRef]
163. Aderneuer, T.; Fernandez, O.; Karpik, A.; Werder, J.; Marhöfer, M.; Kristiansen, P.M.; Ferrini, R. Surface topology and functionality of freeform microlens arrays. *Opt. Express* **2021**, *29*, 5033–5042. [CrossRef]
164. Wang, J.; Li, J.; Wu, Y.F.; Yu, H.W.; Cui, L.B.; Sun, M.; Chiang, P.Y. A 256 × 256 LiDAR Imaging System Based on a 200 mW SPAD-Based SoC with Microlens Array and Lightweight RGB-Guided Depth Completion Neural Network. *Sensors* **2023**, *23*, 6927. [CrossRef]
165. Speck, H.; Munkelt, C.; Heist, S.; Kühmstedt, P.; Nori, G. Efficient freeform-based pattern projection system for 3D measurements. *Optics Express* **2022**, *30*, 39534–39543. [CrossRef] [PubMed]
166. Cheng, Y.; Liu, K.; Wang, Z.C.; Xu, H.Y.; Lu, Y.B. Design and manufacturing technology of ultrashort-throw projectors with freeform mirrors. *Opt. Eng.* **2022**, *61*, 125104. [CrossRef]
167. Zhou, X.R.; Xue, C.X.; Wie, Y.M. Design of a freeform illumination structure for digital display projection. *Appl. Opt.* **2025**, *64*, 4582–4588. [CrossRef]
168. Jeon, H.S.; Kim, Y.M.; Hahn, J.K. Aberration-free warp projection on a horopter screen using freeform holographic optical elements. *Opt. Express* **2023**, *31*, 7466–7479. [CrossRef]

169. Wang, D.; Cheng, D.W.; Liu, Y.; Shan, Y.F.; Sun, J.P.; Wang, X.M.; Wang, Y.T. Development of a wide-field-of-view head-mounted display utilizing freeform surfaces for oblique projection. *Opt. Express* **2025**, *33*, 32209–32226. [CrossRef]
170. Wang, X.M.; Cheng, D.W.; Shan, Y.F.; Wang, D.; Yang, T.; Wang, Y.T. Design of Compact Liquid Crystal on Silicon Projection Optics Utilizing a Common Freeform Optical Path for Augmented Reality Displays. *Adv. Intell. Syst.* **2026**, *8*, 2500014. [CrossRef]
171. Cvach, B.; Acosta, E.; Arines, J.; González Amodor, E.; Kim, Y.-J.; Park, S.-K.; Bog, M.-G.; Blanc, D.; Joannes, L.; Kim, D.W. Focus-invariant presbyopia-correcting phase optics design and optimization. *Proc. SPIE* **2025**, *13596*, 1359604.
172. Yen, C.-T.; Jin, S.-C. Freeform Surface Lens Design Using Genetic Algorithm with Acrylic Material for Reducing Aberrations in Multifocal Artificial Intraocular Lens to Enhance Image Sensing Quality. *Sens. Mater.* **2022**, *34*, 187–201. [CrossRef]
173. Alió, J.L.; Rombach, M.C. The Lumina Accommodative Intraocular Lens. In *Multifocal Intraocular Lenses*; Alió, J.L., Pikkel, J., Alió del Barrio, J.L., Eds.; Springer: Cham, Switzerland, 2026; pp. 505–516.
174. Bissen-Miyajima, H.; Midorikawa, M.; Fujisaki, R.; Ota, Y.; Minami, K.; Honda, R. Early clinical results of a newly developed continuous range of vision intraocular lens. *Ophthalmol. Ther.* **2025**, *14*, 2937–2945. [CrossRef]
175. Kang, S.J.; Arsenault, S.M.; O'Brian, R.C.; Chatzea, M.S.; Zarei-Ghanavati, S.; Beniz, L.A.F.; Yoo, S.H. Comparison of Visual Performance and Patient Satisfaction Between Two Trifocal Intraocular Lenses: A Prospective, Paired-Eye Comparative Study. *Clin. Ophthalmol.* **2026**, *20*, 572237. [CrossRef]
176. Simpson, M.J.; Gatinel, D.; Faria-Ribeiro, M.; Wei, X.; Yoon, G.Y.; Liang, Z.Z.; Artal, P.; Marcos, S. Design concepts for advanced-technology intraocular lenses [Invited]. *Biomed. Opt. Express* **2025**, *16*, 334–361. [CrossRef]
177. Li, L.; Yi, A.Y. Design and fabrication of a freeform microlens array for a compact large-field-of-view compound-eye camera. *Appl. Opt.* **2012**, *51*, 1843–1852. [CrossRef]
178. Galvez, D.; Hong, Z.H.; Rocha, A.D.; Heusinkveld, J.M.; Ye, P.R.; Liang, R.G.; Barton, J.K. Characterizing close-focus lenses for microendoscopy. *J. Opt. Microsyst.* **2023**, *3*, 011003. [CrossRef] [PubMed]
179. Zou, Y.C.; Chau, F.S.; Zhou, G.Y. Ultra-compact optical zoom endoscope using solid tunable lenses. *Opt. Express* **2017**, *25*, 20675–20688. [CrossRef]
180. Huang, L.H.; Huang, Z.Y.; Liu, D.J.; Su, C.Y.; Tai, Y.L.; Wang, M.; Wang, Y.; Wang, Y.P.; Liao, C.R. Full-color imaging with a 3D nanoprinted fiber endoscope. *Opt. Lett.* **2026**, *51*, 37–40. [CrossRef] [PubMed]
181. Hou, C.L.; Yu, Y.; Zhang, D.B.; Liu, X.; Jin, K.K.; Shi, Z.; Zhao, J.F.; Cui, G.M. Miniature wide angle optical system with freeform lens. *Opt. Rev.* **2024**, *31*, 497–508. [CrossRef]
182. Li, Y.F.; Li, Z.X.; Wang, T.C.; Tao, S.P.; Zhang, D.F.; Ren, S.H.; Ma, B.; Zhang, C.H. Research on the Design and Alignment Method of the Optic-Mechanical System of an Ultra-Compact Fully Freeform Space Camera. *Sensors* **2023**, *23*, 9399. [CrossRef]
183. Bauer, A.; Rolland, J.P.; Clark, S.; Potma, E.; Hanninen, A. All-reflective freeform microscope objective for ultra-broadband microscopy. *Opt. Express* **2024**, *32*, 47893–47907. [CrossRef]
184. Weniger, D.; Serna, S.; Ranno, L.; Kimerling, L.; Agarwal, A. Advances in waveguide to waveguide couplers for 3D integrated photonic packaging. *Light Sci. Appl.* **2026**, *15*, 17. [CrossRef]
185. Yu, S.L.; Ranno, L.; Du, Q.Y.; Serna, S.; McDonough, C.; Fahrenkopf, N.; Gu, T.; Hu, J.J. Free-Form Micro-Optics Enabling Ultra-Broadband Low-Loss Off-Chip Coupling. *Laser Photonics Rev.* **2023**, *17*, 2200025. [CrossRef]
186. Yu, S.L.; Ranno, L.; Du, Q.Y.; Sema, S.; McDonough, C.; Fahrenkopf, N.; Gu, T.; Hu, J.J. Ultra-broadband, high-efficiency, and wafer-scale fiber-to-chip coupling using free-form micro-optical reflectors. *Proc. SPIE* **2022**, *12006*, 1200604.
187. Dietrich, P.-I.; Blaicher, M.; Reuter, I.; Billah, M.; Hoose, T.; Hofmann, A.; Caer, C.; Dangel, R.; Offrein, B.; Troppenz, U.; et al. In situ 3D nanoprinting of free-form coupling elements for hybrid photonic integration. *Nat. Photonics* **2018**, *12*, 241–247. [CrossRef]
188. Xu, Y.L.; Maier, P.; Trappen, M.; Dietrich, P.-I.; Blaicher, M.; Jutas, R.; Weber, A.; Kind, T.; Dankwart, C.; Stephan, J.; et al. 3D-printed facet-attached microlenses for advanced photonic system assembly. *Light Adv. Manufact.* **2023**, *4*, 3. [CrossRef]
189. Su, C.Y.; Li, Z.R.; Liu, D.J.; Huang, Z.Y.; Tai, Y.L.; Huang, L.H. Spatial Beam Intensity Shaping Based on an On-Fiber 3D Nanoprinted Microlens. *J. Light. Technol.* **2025**, *43*, 3968–3973. [CrossRef]
190. Missine, J.; Verplancke, R.; Chang, Y.-T.; van Steenberge, G. Microlenses on photonic integrated circuits enable flexible packaging and optical isolator integration. *Opt. Laser Technol.* **2025**, *189*, 112940. [CrossRef]
191. Berto, P.; Philippet, L.; Osmond, J.; Liu, C.F.; Afridi, A.; Marques, M.M.; Agudo, B.M.; Tessier, G.; Quidant, R. Tunable and free-form planar optics. *Nat. Photonics* **2019**, *13*, 649–656. [CrossRef]
192. Rothermel, F.; Thiele, S.; Jung, C.; Giessen, H.; Herkommer, A. Towards magnetically actuated 3D-printed micro-optical elements. *Proc. SPIE* **2021**, *11816*, 1181601.
193. Calikoglu, A.; Lux, F.; Taege, Y.; Zappe, H.; Ataman, C. 3D Nano-Printed Bistable Microlens Actuator for Reconfigurable Micro-Optical Systems. *Adv. Funct. Mater.* **2024**, *34*, 2408867. [CrossRef]
194. Rothermel, F.; Toulouse, A.; Thiele, S.; Jung, C.; Drozella, J.; Steinhoff, R.; Giessen, H.; Herkommer, A.M. Magnetically actuatable 3D-printed endoscopic microsystems. *Commun. Eng.* **2025**, *4*, 69. [CrossRef]
195. Petsch, S.; Grewe, A.; Köbele, L.; Sinzinger, S.; Zappe, H. Ultrathin Alvarez lens system actuated by artificial muscles. *Appl. Opt.* **2016**, *55*, 2718–2723. [CrossRef]

196. Li, S.B.; Liu, L.; Xing, H.Y.; Li, Z.H.; Cheng, Y. Adaptive Varifocal Lenses Based on Dielectric Elastomer Actuator. *Photonics* **2025**, *12*, 227. [CrossRef]
197. Nocentini, S.; Martella, D.; Parmeggiani, C.; Wiersma, D.D. 3D Printed Photoresponsive Materials for Photonics. *Adv. Opt. Mater.* **2019**, *7*, 1900156. [CrossRef]
198. Rondelez, N.; Desnijder, K.; Ryckaert, W.; Meuret, Y. Programmable freeform optics with extended white light sources: Possibilities and limitations. *Opt. Express* **2023**, *31*, 1303–1317. [CrossRef] [PubMed]
199. Gu, T.; Kim, H.J.; Rivero-Baleine, C.; Hu, J.J. Reconfigurable metasurfaces towards commercial success. *Nat. Photonics* **2023**, *17*, 48–58. [CrossRef]
200. Pribosek, J.; Bainschab, M.; Sasaki, T. Varifocal MEMS mirrors for high-speed axial focus scanning: A review. *Microsyst. Nanoeng.* **2023**, *9*, 135. [CrossRef]
201. Han, Z.Y.; Colburn, S.; Majumdar, A.; Böhringer, K.F. Millimeter-scale focal length tuning with MEMS-integrated meta-optics employing high-throughput fabrication. *Sci. Rep.* **2022**, *12*, 5385. [CrossRef]
202. Sun, Y.H.; Deng, C.Y.; Xie, Z.H.; Huang, L.; Hu, G.H.; Yun, B.F.; Cu, Y.P. Compact, easy-accessible and tunable double injection micro-ring element for real-time spectral reshaping. *Opt. Comm.* **2023**, *542*, 129546. [CrossRef]
203. Chen, L.J.; Liang, S.J.; Chen, Z.S.; Liang, X.F.; Chen, Q.M. Electrically Tunable Lenses for Imaging and Light Manipulation. *Micromachines* **2023**, *14*, 319. [CrossRef]
204. Santonocito, A.; Patrizi, B.; Toci, G. Recent Advances in Tunable Metasurfaces and Their Application in Optics. *Nanomaterials* **2023**, *13*, 1633. [CrossRef]
205. Hu, S.Q.; Park, C.; Jeong, S.; Jeon, N.; Kim, J.T.; Rho, J.S. Additive manufacturing of metastructures at the micro- and nano-scale. *Chem. Soc. Rev.* **2026**, *55*, 1666–1716. [CrossRef]
206. Pruessner, M.W.; Tyndall, N.F.; Stievater, T.H. MEMS-tunable polarization management in photonic integrated circuits. *Opt. Express* **2023**, *31*, 31316–31328. [CrossRef] [PubMed]
207. Minano, J.C.; Benítez, P.; Chaves, J.; Duerr, F. Freeform optics. *Progr. Opt.* **2022**, *67*, 1–124.
208. Nie, Y.F.; Zhang, J.G.; Su, R.M.; Ottevaere, H. Freeform optical system design with differentiable three-dimensional ray tracing and unsupervised learning. *Opt. Express* **2023**, *31*, 7450–7465. [CrossRef]
209. Keawmuang, H.; Hu, S.Q.; Badloe, T.; So, S.N.; Rho, J.S. Hybrid Frameworks Integrating Deep Learning and Optimization Methods for Inverse Design in Nanophotonics. *ACS Appl. Mater. Interfaces* **2025**, *17*, 33259–33270. [CrossRef] [PubMed]
210. Wu, W.C.; Zhu, J. Optical design mode based on fast automatic design process for freeform reflective imaging systems with modest FOV. *Opt. Express* **2023**, *31*, 40952–40968. [CrossRef] [PubMed]
211. Shi, H.D.; Zhao, H.; Wang, J.Y.; Zhang, Y.-L.; Wu, Y.F.; Wang, C.; Fu, Q.; Jiang, H.L. Analysis and experiment of polarization characteristics of Off-axis freeform optical system. *Opt. Laser Technol.* **2023**, *163*, 109383. [CrossRef]
212. Wang, Y.K.; Wang, J.J.; Guo, P. Generic fabrication solution of freeform Fresnel optics using ultra-precision turning. *Opt. Express* **2023**, *31*, 44622–44647. [CrossRef]
213. ten Thije Boonkkamp, J.H.M.; Mitra, K.; Anthonissen, M.J.H.; Kusch, L.; Braam, P.A.; Ijzerman, W.L. Inverse freeform design in non-imaging optics: Hamilton's theory of geometrical optics, optimal transport, and least-squares solvers. *Front. Phys.* **2025**, *13*, 1518660. [CrossRef]
214. Kumar, S.; Zhong, W.B.; Scott, P.; Jiang, X.Q.; Zeng, W.H. Aberration control-based design for freeform monolith. *Proc. CIRP* **2024**, *128*, 262–267. [CrossRef]
215. Yu, J.D.; Mao, X.L. Design of Off-Axis Four-Mirror Optical Systems Enabled by Freeform Optics. *Photonics* **2025**, *12*, 107. [CrossRef]
216. Zhang, Z.J.; Fang, L.Y.; Ding, Z.H.; Guo, F.X.; Shi, J.C.; Wu, R.M. Tailoring freeform off-axis reflective beam shaping systems. *Opt. Lasers Eng.* **2025**, *184*, 108665. [CrossRef]
217. Xu, H.M.; Yang, T.; Cheng, D.W.; Wang, Y.T. Compact freeform near-eye display system design enabled by optical-digital joint optimization. *Front. Phys.* **2024**, *12*, 1440129. [CrossRef]